Monthly Notices
of the
ROYAL ASTRONOMICAL SOCIETY

MNRAS **440,** 3444–3461 (2014) doi:10.1093/mnras/stu529

Temperaments of young stars: rapid mass accretion rate changes in T Tauri and Herbig Ae stars

G. Costigan,[1,2,3★] Jorick S. Vink,[2] A. Scholz,[1,4] T. Ray[1] and L. Testi[3,5,6]

[1]*School of Cosmic Physics, Dublin Institute for Advanced Studies, 31 Fitzwilliam Place, Dublin 2, Ireland*
[2]*Armagh Observatory, College Hill, Armagh BT61 9DG, Northern Ireland*
[3]*European Southern Observatory, Karl-Schwarzschild-Str. 2, D-85748 Garching bei München, Germany*
[4]*School of Physics and Astronomy, University of St. Andrews, North Haugh, St Andrews KY16 9SS, Scotland*
[5]*INAF-Osservatorio Astrofisico di Arcetri, Largo E. Fermi, I-50125 Firenze, Italy*
[6]*Excellence Cluster Universe, Boltzmannstr. 2, D-85748 Garching, Germany*

Accepted 2014 March 13. Received 2014 March 13; in original form 2013 June 6

ABSTRACT

Variability in emission lines is a characteristic feature in young stars and can be used as a tool to study the physics of the accretion process. Here, we present a study of Hα variability in 15 T Tauri and Herbig Ae stars (K7 - B2) over a wide range of time windows, from minutes, to hours, to days, and years. We assess the variability using linewidth measurements and the time series of line profiles. All objects show gradual, slow profile changes on time-scales of days. In addition, in three cases there is evidence for rapid variations in Hα with typical time-scales of 10 min, which occurs in 10 per cent of the total covered observing time. The mean accretion rate changes, inferred from the line fluxes, are 0.01–0.07 dex for time-scales of <1 h, 0.04–0.4 dex for time-scales of days, and 0.13–0.52 dex for time-scales of years. In Costigan et al., we derived an upper limit finding that the intermediate (days) variability dominated over longer (years) variability. Here, our new results, based on much higher cadence observations, also provide a *lower* limit to accretion rate variability on similar time-scales (days), thereby constraining the accretion rate variability physics in a much more definitive way. A plausible explanation for the gradual variations over days is an asymmetric accretion flow resulting in a rotational modulation of the accretion-related emission, although other interpretations are possible as well. In conjunction with our previous work, we find that the time-scales and the extent of the variability is similar for objects ranging in mass from $\sim$0.1 to $\sim$5 $M_\odot$. This confirms that a single mode of accretion is at work from T Tauri to Herbig Ae stars – across a wide range of stellar masses.

Key words: accretion, accretion discs – stars: pre-main-sequence.

1 INTRODUCTION

Accretion is a vital and central process in the formation of low-mass stars, controlling the flow of angular momentum and mass from the interstellar medium on to the star. The accretion history can have a large effect on the long-term properties of the stellar system, such as its luminosity, radius, mass, and rotation rate (Baraffe, Chabrier & Gallardo 2009). It is also thought to be strongly connected to the mechanisms of wind and jet launching (Ray et al. 2007), and of disc clearing and evolution (Muzerolle et al. 2005). In order to understand these processes, we need to gain a full understanding of accretion.

The current model for this process is magnetospheric accretion where the stellar magnetic field threads the disc, and the material in the disc falls along the field lines on to the surface of the star (Königl 1991). However, this simple model does not explain one of the defining features: its variability. The accretion flows and shocks emit continuum emission from the ultraviolet (UV) to the infrared (IR) as well as a number of emission lines (e.g. Hα, Ca II, He I), which, when observed are all found to be variable on time-scales from hours, to weeks, and to years (Mohanty, Jayawardhana & Basri 2005; Scholz & Jayawardhana 2006; Nguyen et al. 2009).

This variability can and has been used to probe the inner regions of these accreting systems, to find the source of the variations and to provide stringent constraints on the nature of the accretion process itself (Dupree et al. 2012). The time-scale of accretion variations and the magnitude of the variations will depend on their source, so by monitoring these accreting systems over different time-scales, we

★E-mail: costigag@tcd.ie

can identify where these variations originate. This has been done very successfully for individual objects such as AATau (Bouvier et al. 2003) and V2129 (Alencar et al. 2012), but it has yet to be done systematically for a larger sample.

Our previous observing program LAMP (Long-term Accreting Monitoring Program) was designed to systematically explore the possible origin of accretion variability by monitoring Hα and the Ca II triplet. Two successful runs took place over two months, with a total baseline of 15 months. Over this period 25 young stellar objects (YSOs) in Chameleon I were observed, each object 12 times. Among these targets, we found 10 accretors, which covered a spectral range of G2–M5.75. All the accretors showed variations in their accretion signatures. The average accretion spread as calculated from the Hα equivalent width (EW), was found to be 0.37 dex (Costigan et al. 2012). Although there are long-term accretion rate variations in the sample, the amplitude of variations reached a maximum or are within 70 per cent of the maximum after 25 d. This was the shortest time-scale in our sample, which indicates the dominant cause of this variability is occurring on times scales of 2–3 weeks, or less.

This result is backed up by other studies, such as a short-term monitoring covering time-scales up to $\sim$48 h of $\sim$29 sources in Chameleon II, which defined the spread in accretion rates as derived from Hα to be 0.2–0.6 dex (Biazzo et al. 2012). Also, Nguyen et al. (2009) found a very similar accretion rate spread over time-scales of days and months. These and our previous results rule out origins of variability such as those due to a wind form the disc or large-scale instabilities in the accretion disc, as these would occur on much longer time-scales of months and years.

These time-scales of $\lesssim$2–3 weeks are close to the rotation period of these kinds of objects (1–10 d; Herbst et al. 2007), which suggests that what we are observing could be a rotational modulation of the accretion flow. If there is even a slight offset between the rotation and the magnetic field axis (2–5°), it has been shown that an asymmetric accretion flow will form (Romanova et al. 2003). As this rotates with the star, different parts of the accretion flow will become visible, which will change the accretion signatures that we observe.

A second possible explanation for variations on these time-scales concerns the existence of instabilities in these systems, either in the magnetic field, or in the inner disc (Gullbring et al. 1998; Kurosawa & Romanova 2013). These will cause short-term, stochastic variations occurring on the time-scales as short as hours.

If we wish to distinguish between these two possible causes of accretion variations on short time-scales, we need to monitor these systems on time-scales close to the rotation period (multiple days) as well as on time-scales of hours. Just such a test can be performed using the high S/N, high-cadence linear spectropolarimetry data set of Vink et al. (2005) on a sample of T Tauri and Herbig Ae stars. This data set will allow us to constrain whether the mass accretion rate variations indeed involve a slow and gradual variation in accretion emission across the rotation period, or if they concern stochastic and rapid variations.

Our combined sample of T Tauri and Herbig Ae stars probing the time-scales of minutes and hours, with LAMP probing the time-scales of days, months, and years, we can constrain the dominant accretion variations. Using the Hα emission as an accretion indicator, and to measure accretion rates, we compare the variations found on all time-scales.

Furthermore, we can extend our work to higher stellar masses (up to 2–3 $M_\odot$ for Herbig Ae stars). This way, we can test whether the accretion process in Herbig Ae stars might be similar to that in lower mass T Tauri stars, as suggested by (Natta et al. 2001; Vink et al. 2002, 2003; Eisner et al. 2004; Garcia Lopez et al. 2006). Whilst magnetic fields have indeed been claimed in Herbig Ae stars (Hubrig, Schöller & Yudin 2004; Wade et al. 2005), the fact that the field incidence in Herbig Ae stars is similarly low to that in post-main-sequence objects (e.g. Alecian et al. 2012) may cast doubt on an extension of the magnetospheric accretion scenario towards higher masses. Therefore the issue of the fundamental accretion process in Herbig Ae stars remains open, and can be tested in this paper.

The paper is laid out as follows: In Section 2, we discuss the chosen sample, the observations and reduction, Section 3 presents the data and the variations present in the Hα emission, Section 4 addresses the nature of the Hα emission, Section 5 discuses the derivation of accretion rates and Section 6 deals with possible causes of the variations observed. Individual sources and their variations are presented in the Appendix.

2 SAMPLE AND OBSERVATIONS

Our targets were originally observed for a linear spectropolarimetry study (Vink et al. 2005) to probe the circumstellar structures around Herbig Ae/Be and T Tauri stars. The sample was chosen from Herbig & Bell (1988), based on their relative brightness ($V \lesssim 11$), and their position on the sky, but not on any known circumstellar geometries, or T Tauri/Herbig Ae type. The target list is provided in Table 1 and the stellar parameters are listed in Table 2.

The observations were obtained during the nights of 2003 December 10–13 and 2001 December 26–27 with the Intermediate dispersion Spectrograph and Imaging System (ISIS) spectrograph on the 4.2 m William Herschel Telescope, La Palma. Each target was monitored over $\lesssim$1 h blocks, in a few cases, targets were observed in multiple blocks in a single night. The number of exposures in each block of observations, the exposure times, and dates of observations are all given in Table 2. A slit width of 1.0 arcsec was used for all observations, along with the Marconi2 CCD detector, and the R1200R grating. This grating has a spectral range of 1000 Å centred on 6500 Å, with a spectral resolution of $\simeq$35 kms^{-1} around Hα. The ISIS set-up also included the polarization optics of a rotating half-wave plate and a calcite block.

The data reduction was carried out using IRAF and included bias-subtraction, spectrum extraction, and wavelength calibrations. Since these spectra were originally used for polarimetry studies, each observation is split into two spectra, of two separate polarizations. The sum of the two extracted spectra were taken as the full Hα emission line and continuum was then normalized to 1 before any measurements were taken.

3 BEHAVIOUR OF THE Hα EMISSION

In the following section, AB Aur is used to represent the typical behaviour of the line emission in the sample. This section will concentrate on the 2003 observations of this object as an example, all of the observations for the remaining 13 targets and the 2001 observations of AB Aur are discussed in the Appendix.

3.1 Hα Profiles

For each block of observations of each object, there are about 20 different exposures over the course of $\sim$1 h (see Table 1). This provides us with very close temporal coverage of the Hα emission. The top row in Fig. 1 shows a time series of profiles across the four nights of observations for AB Aur in 2003. These four nights were

Table 1. Target list. Magnitudes are given in the *V* band. Variations in *V* band are given where found in the literature. The T Tauri type is taken from Herbig & Bell (1988), where an SU Aur type is given as 'A star like SU Aur: type late F to K, weak emission at Hα and Ca II, very broad absorption lines ($v \sin i > 50$ km s^{-1}), and relatively high luminosity'. Exposures are given as number of exposures times the exposure time in seconds. References: (1) Mora et al. (2001), (2) Høg et al. (2000), (3) Cohen & Kuhi (1979), (4) Rydgren, Strom & Strom (1976), (5) Jaschek, Jaschek & Andrillat (1988), (6) Herbig & Bell (1988), (7) Basri & Bertout (1989), (8) Grankin et al. (2008), (9) Cody et al. (2013), (10) de Winter et al. (2001), (11) Rydgren & Vrba (1983), (12) Davies et al. (1990).

Name	Magnitude	ΔMagnitude	SpT	Reference	Type	Date	Exposures	Total (h)
RY Tau	10.1	9.55–11.56	K1	3, 8	CTTS	2001-12-26	4×120, 12×180	4.0
						2003-12-10	8×120, 20×240	
						2003-12-12	8×90, 12×180	
						2003-12-13	8×120, 12×180	
AB Aur	7.1	± 0.7	A0	3, 9		2001-12-27	20×30, 16×30, 16×30	1.83
						2003-12-10	12×90	
						2003-12-11	20×60	
						2003-12-12	20×60	
						2003-12-13	4×120, 12×90	
T Tau	10.3	9.75–10.18	K1	3, 8	CTTS	2001-12-12	8×45, 16×120	1.37
						2003-12-12	4×60, 18×150	
SU Aur	9.0	8.92–10.02	G2	3, 8	SU AUR	2001-12-27	12×180	2.30
						2003-12-10	8×90,16×150	
						2003-12-11	4×90, 5×240	
						2003-12-13	12×120	
DR Tau	11.43	10.76–12.78	K5	2, 1, 8	CTTS	2001-12-27	16×180	1.87
						2003-12-12	4×60, 20×180	
RW Aur A	10.36	9.32–11.75	K1	2, 7, 8	CTTS	2001-12-26	11×180	1.40
						2003-12-10	12×150	
						2003-12-13	4×60, 20×150	
GW Ori	11.1	9.74–10.53	G5	3, 8	CTTS	2003-12-11	4×60, 20×240	1.40
V773 Tau	10.35	10.82–11.03	K2	4, 11	CTTS	2003-12-13	4×60, 16×240	1.13
UX Tau A	11.3	10.64–12.77	K2	3, 8	WTTS	2003-12-13	1×120, 24×240	1.63
BP Tau	12.1	11.67–12.99	K7	3	CTTS	2003-12-12	4×90	2.13
						2003-12-13	4×30, 24×300	
BF Ori	12.2	9.82–11.67	A0	3, 10	HAe	2001-12-27	16×180	0.80
LkHα 215	10.8	10.36–10.47	B1	3, 12	HAe	2001-12-12	16×120	0.53
MWC 480	7.6	–	A3	5	HAe	2001-12-26	16×75, 16×30	1.03
						2001-12-27	16×45, 8×45, 16×60	
CO Ori	9.83	9.81–12.73	F8	6, 8	SU AUR	2001-12-27	8×120, 8×180	
						2001-12-24	8×12, 8×180	1.09

the 10th, 11th, 12th, and 13th of December, and for simplicity these will be referred to Night 1, 2, 3, and 4, respectively. Each profile is off-set from the previous one for clarity. A time stamp is given to the right of each plotted spectrum, and it takes the form of the time difference between the first observation in that block and that spectrum.

The changes in the profiles during Nights 1, 2, and 4, are typical of what is seen in the majority of objects of this sample. These changes will be referred to as slow variations. During each of these nights, AB Aur shows a strong central emission with a large blue-shifted absorption in the wing. Within this blue-shifted absorption, there is also a small emission peak. Within a single night's observation, there is very little change seen within the profile.

Larger changes in the profile can be seen from night to night. For example, in the case of AB Aur, the small emission peak within the blue absorption noticeably changes in wavelength. The strength of the emission, the depth of the absorption, and the red wing also change between the nights observations.

It is only on Night 3 of the observations that we see large changes in the profile from one exposure to the next. These changes occur on the time-scales of minutes, and they take the form of a drop in intensity across the line, and a broadening of the emission. These changes are referred to as rapid events. They are not common in the sample. These rapid events also occur in the spectra of RY Tau and RW Aur; however, they are much weaker than those seen in AB Aur, and show different behaviour.

3.2 Average and variance profiles

In order to better discern where the changes in the emission profiles occur, average and variance profiles are utilized. The average profile in this case is simply the average flux at each wavelength and is calculated for each night of observation separately. The variance (σ) at a wavelength λ is calculated using the following:

$$\sigma^2(\lambda) = \frac{1}{n-1}\sum_{i=1}^{n}(I_{\lambda,i} - \bar{I}_\lambda)^2, \quad (1)$$

where $I_{\lambda,i}$ is the flux at wavelength λ for spectrum number i, $\bar{I}_\lambda$ is the average flux at that wavelength and n is the total number of spectra for a given object (Johns & Basri 1995a). The normalized variance is then given by $\sigma_N^2(\lambda) = \sigma^2(\lambda)/\bar{I}_\lambda$. The variance profile allows us to distinguish which parts of the emission profile are changing, and which are remaining the same.

Table 2. Published stellar parameters. References: (1) Bertout, Basri & Bouvier (1988), (2) Praderie et al. (1986), (3) DeWarf et al. (2003), (4) Bohm & Catala (1993), (5) Mora et al. (2001), (6) Herbst & Layden (1987), (7) Johns & Basri (1995a), (8) Hartmann et al. (1986), (9) Manoj et al. (2006), (10) Kraus & Hillenbrand (2009), (11) Welty (1995), (12) Rydgren & Vrba (1983), (13) Espaillat et al. (2007), (14) Mora et al. (2001), (15) Mannings & Sargent (1997), (16) Catala et al. (1999), (17) Petrov et al. (2001), (18) Hernández et al. (2004), (19) White & Ghez (2001), (20) Gullbring et al. (1998), (21) Mathieu, Adams & Latham (1991), (22) Bouvier et al. (1986), (23) Boden et al. (2007), (24) Kenyon & Hartmann (1995), (25) Bouvier & Bertout (1989), (26) Vrba et al. (1984), (27) Hillenbrand et al. (1992), (28) Calvet et al. (2004), (29) Hubrig et al. (2011), (30) Akeson, Ciardi & van Belle (2003), (31) Fukagawa et al. (2004), (32) Akeson et al. (2002), (33) López-Martín, Cabrit & Dougados (2003), (34) Simon, Dutrey & Guilloteau (2000).

Object	M_* ($M_\odot$)	Teff (K)	R_* ($R_\odot$)	P_{rot} (d)	$v \sin i$ (km s^{-1})	Inclination	Determination of inclination	Reference
RY Tau	2.0	6300	2.7	5.6	55 ± 3	30°	Inteferometric	1, 33, 7, 6, 5
AB Aur	2.5	9332	2.5	1.4	–	30°	*H*-band imaging	2, 4, 5, 31, 16
T Tau	2.0	5250	3.3	2.8	19.5 ± 2.5	29°	Inteferometric	1, 19, 6, 32
SU Aur	2.0	5550	3.1	1.7–2.7	59 ± 1	63°	Inteferometric	1, 3, 7, 6
DR Tau	1.0	4060	1.2	5.1	<10	–	–	1, 20, 7
RW Aur	1.0	4700	2.7	5.6	16–40	45°	Jet Inclination	1, 17, 33
GW Ori	3.7	5700	2.5	3.2	40–43	15°	Inteferometric	9, 21, 22, 10, 25
V773 Tau	1.2	4900	2.4	3.43	41.4	–	–	10, 27, 23, 11, 12
UX Tau	1.3	4900	2.0	2.7	25	50°	Photometry	10, 24, 13, 25
BP Tau	0.8	4000	3.0	7.6	<10	30°	Inteferometric	1, 19, 1, 26, 8, 34
BF Ori	2.5	8912	1.3	–	37 ± 2	–	–	9, 27, 14
LkHα 215	4.8	14125	5.4	–	<200	–	–	18, 9, 27
MWC 480	2.3	8890	2.1	0.5	90	30°	Interferometric	15, 29, 15
CO Ori	2.5	6030	4.3	–	40–50	–	–	28

The average and normalized variance profiles for AB Aur are given in the second row of Fig. 1. The horizontal dashed line in these plots represents the zero variability level which is given by

$$\sigma_N^2(\lambda) = \sigma_{N,0}^2 \left(\frac{\sqrt{\bar{I}_\lambda}}{\bar{I}_\lambda} \right)^2, \quad (2)$$

where $\sigma_{N,0}^2$ is the normalized variance in the continuum (Scholz & Jayawardhana 2006; Stelzer, Scholz & Jayawardhana 2007). The zero variability level can be considered the level below which variations are not significant. The area in the variance profile above the zero-variability level, i.e. significant peaks of variations are shown as a filled (blue) colour.

Across the four nights, there different parts of the Hα profile change. A constant change in intensity across the entire line would result in a variance profile that had the same shape as the emission profile. However, for AB Aur, there are distinct structures within the variance profile for each night.

For Nights 1 and 2, the changes are concentrated in the wings of the profile. This behaviour is representative of the slow variations seen in the majority of the sample, where most of the changes occur in the line wings rather than the line centre.

On the third night of observations, the rapid variations noted in the time series of the Hα profile manifest themselves as three distinct regions of variations: one peak in the blue wing, one peak in the line centre, and another one in the red wing. (Note the scale change for the variance profile on the third night.) This is unusual behaviour within this sample, these large changes are only seen in three observation blocks for three separate objects over the course of these observations. However, no other object shows such strong, distinct peaks in the variance profile as AB Aur.

3.3 Distinguishing variations

The majority of the variations in the profiles are small. So in order to perceive these changes more clearly, differential surface plots and differential time series of the profiles are given for each observation block. (See third and fourth row of Fig. 1.) The surface plots were created by finding the difference between the first spectrum of that observation block and all the preceding spectra. These are then plotted as a surface where the difference in flux is colour coded. As you move from the bottom of the plot to the top, you are moving through the observation block, and the changes in the surface plot correspond to the differential changes in the profiles across the block.

The last row in Fig. 1, represents cuts across these surface plots. As with the profiles given in the top-left panels, the time stamp shows the difference in minutes between the first observation in that block and that spectrum.

3.4 Line measurements

In order to quantify the changes in the Hα emission, two measurements of the emission line were taken, the Hα EW, and the Hα 10 per cent width (10 w). The Hα EW gives a measure of the strength of the emission line, which is measured in Å and is given by the following:

$$\mathrm{EW} = \sum \frac{F_c - F_\lambda}{F_c} \Delta\lambda, \quad (3)$$

where F_c is the continuum flux, and F_λ is the flux at wavelength λ. The Hα 10 w is simply the full width of the line at 10 per cent of the peak height, where the units are km s^{-1}.

The integration windows for each source differ and are chosen on the basis of the breadth of the Hα emission. The window size for each object is given in Table 4, along with the average, max, min, and standard deviation of both the Hα EW and 10 w measurements.

From these measurements, it can be noted that the slow variations observed across the entire sample do result in small changes in the EW and the 10 w. Much more significant variations occur between each night's observations.

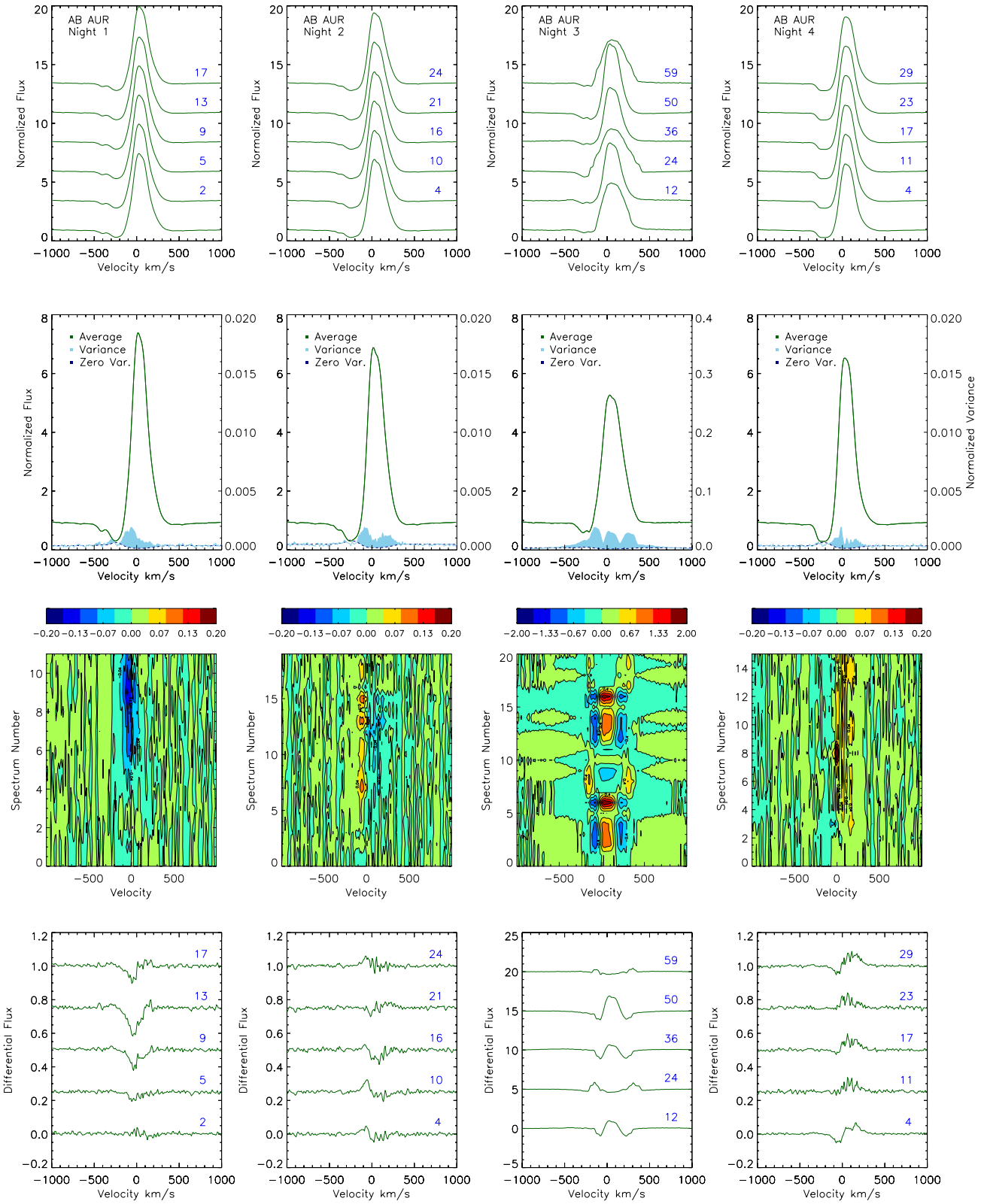

Figure 1. First row: sample of Hα profiles across the fur nights of observations of AB Aur in 2003. Each profile is off-set from the previous one for clarity. A time stamp is given to the right of each plotted spectrum, and it takes the form of the time difference between the first observation in that block and that spectrum. Second row: average and variance profiles. Third row: a differential surface plot. This plot shows the colour-coded difference between the first spectra of that night and the preceding spectra. Note scale change on third night. Fourth row: time series of cuts in differential flux plots. This was done in the same way as the surface plots, where the first spectrum of that night was removed from all the rest of the spectra. These are the same profiles as chosen for the profile time series.

Table 3. Average Hα EW and 10 w measurements for 2001 observations. Also given are the max, min measurements, and the standard deviations (σ) across the range of measurements. Window is the integration window over which EW and 10 w were calculated. No 10 w measurements are given for MWC 480 as the entire blue wing is in absorption.

Object	Night	$\overline{\text{EW}}$ (Å)	Maximum	Minimum	σ	Er.	$\overline{10\,w}$ (km s^{-1})	Maximum	Minimum	σ	Win (Å)
RY Tau	ALL	10.38	10.64	10.21	0.12	(0.08)	650	660	640	6	25
AB Aur	ALL	24.80	26.81	24.80	0.56	(0.28)	360	360	350	4	25
	1	26.55	26.81	26.35	0.14		360	360	355	2	
	2.1	25.89	26.36	25.60	0.16		360	360	350	4	
	2.2	25.81	26.03	25.51	0.17		360	360	360	0	
	2.3	24.97	25.15	24.80	0.11		360	360	350	4	
T Tau	ALL	71.42	86.51	55.96	12.22	(0.55)	520	525	510	6	25
	1	86.10	86.51	85.79	0.18		520	525	510	8	
	2	61.64	64.28	55.96	1.93		515	525	510	4	
SU Aur	ALL	4.65	5.43	3.91	0.69	(0.08)	550	560	535	6	20
	1	3.98	4.05	3.93	0.04		555	560	545	5	
	2	5.33	5.43	5.24	0.06		545	555	535	7	
DR Tau	ALL	65.32	78.69	58.50	7.53	(0.68)	659	689	625	20	25
	1	78.16	78.69	77.49	0.43		685	690	670	8	
	2	61.31	63.45	58.50	1.86		650	680	625	15	
RW Aur	ALL	74.04	81.11	67.88	3.95	(3.6)	720	725	715	5	40
GW Ori	ALL	19.33	19.52	19.06	0.14	(0.16)	505	505	490	6	25
BF Ori	ALL	3.88	4.21	3.44	0.23	(0.86)	495	505	490	5	25
LkHα 215	ALL	30.45	30.72	29.87	0.22	(0.22)	690	700	680	5	30
MWC480	ALL	11.85	15.11	9.65	1.87	(0.36)	–	–	–	–	30
	1	11.21	11.74	10.48	0.37		–	–	–	–	
	2	10.53	11.54	9.65	0.74		–	–	–	–	
	3	14.86	15.11	14.65	0.13		–	–	–	–	
	4	10.71	11.75	9.85	0.78		–	–	–	–	
CO Ori	ALL	7.57	7.91	7.22	0.19	(0.1)	585	600	560	10	20

Error analysis was performed by varying the measurement parameters for the EW. The integration window was varied by ±0.5, 1, 1.5, 2, 2.5, 3 Å and continuum measurements were varied by ±1, 2, 3 σ. The mean differences between each of these variations and the 'real' measurement were added in quadrature. The square root of this sum was taken as the error estimate for that spectrum. This was performed on a sub-sample of spectra for each object, and then averaged across the sub-sample of spectra to give an estimate of the errors in the EW measurements. The 10 w is not as sensitive to these parameter variations as the EW is, and it is more difficult to get a proper estimate of the measurement errors using this method. In this case, twice the spectral resolution (10 km s^{-1}) can be taken as a rough estimate of the 10 w errors. These measurement errors are given in Tables 3 and 4.

3.5 Plausibility checks

In order to determine whether the slow variations observed in the sample are real changes within the line profile a number of tests were performed and are listed below.

(i) The changes in the line measurements were compared to the changes in the signal-to-noise (S/N) in each observations. In the majority of cases, the changes in the EW or 10 w do not follow the changes in the S/N. There is one object, RY Tau for which changes in the intensity across the line correspond to changes in the S/N (see Appendix, Fig. A7). This occurs in the first night's observations in 2003, but there is a similar change in S/N during the second night without any corresponding change to the EW measurement, so the two events are not considered to be connected.

(ii) With regards to the rapid events in the profile of AB Aur, tests were also run on the sky subtraction around Hα. This was found not to be the cause of these changes.

(iii) Instrumental set-up was checked for any changes between observations, no differences were found. The dispersion axis changed between the 2001 and 2003 observations, and as a result the wavelength range is smaller (∼200 Å) in the 2001 observations. However, this does not affect our observations of the Hα emission line.

(iv) There were changes in the weather conditions across the four nights, but these would result in a change in the intensity across the entire profile rather than a change in the profile structure.

(v) The stability of the instrument was tested with a number of objects and using the changes due to telescope flexure (15 μm h^{-1}) compared to the pixel size.[1] In the 2001 observations, the pixel size is 24 μm and in the 2003 observations, the pixel size is 13.5 μm. The difference arises from a change in detector. Based on this, a drift rate of 1 pixel h^{-1} was used to estimate how this would affect our line profiles. For some objects, the morphology of the variance profile and the appearance of the surface plot in the shifted series of spectra are very similar to what is observed. In the cases tested, though the difference in flux in the lines matched that observed, the variance profiles remained lower than the observed variance profiles. Also any changes in the EW were well below those observed for these sequences, and remained within the experimental error. The top panels of Fig. 2, show the observed variations in DR Tau in 2003. By shifting the spectra by a total of 1 pixel h^{-1} (as expected from

[1] See http://www.ing.iac.es/Astronomy/instruments/isis/flextest.html.

Table 4. Average Hα EW and 10 w measurements for 2003 observations. Also given are the max, min measurements, and the standard deviations (σ) across the range of measurements. Window is the integration window over which EW and 10 w were calculated.

Object	Night	$\overline{\text{EW}}$ (Å)	Maximum	Minimum	σ	Er.	$\overline{10\,w}$ (km s^{-1})	Maximum	Minimum	σ	Win (Å)
RY Tau	ALL	17.62	24.52	14.85	3.59	(0.11)	670	710	640	18	25
	1	23.08	24.52	20.37	1.43		690	710	680	8	
	2	14.98	15.16	14.85	0.11		675	680	665	4	
	3	15.90	16.02	15.73	0.08		655	660	640	5	
AB Aur	ALL	22.87	25.92	19.99	1.84	(0.21)	385	550	340	54	25
	1	25.56	25.92	25.30	0.21		370	370	370	0	
	2	23.65	23.78	23.47	0.09		360	360	360	0	
	3	22.72	23.49	21.17	0.60		445	550	345	62	
	4	20.10	20.26	19.99	0.08		345	345	340	2	
T Tau	ALL	47.03	48.02	46.51	0.47	(0.39)	445	450	445	2	25
SU Aur	ALL	5.71	8.09	3.60	1.91	(0.09)	575	610	540	23	20
	1	7.96	8.09	7.56	0.13		590	600	580	4	
	2	4.34	4.49	3.93	0.16		550	565	540	6	
	3	3.68	3.95	3.60	0.09		560	610	585	8	
DR Tau	ALL	80.48	81.47	78.74	0.70	(0.29)	640	645	630	5	50
RW Aur	ALL	64.66	77.13	34.57	13.54	(3.18)	720	740	705	9	40
	1	48.54	52.32	36.57	3.67		730	740	720	5	
	2	75.41	77.13	73.34	0.93		715	720	705	5	
GW Ori	ALL	33.16	33.32	32.99	0.07	(0.12)	405	410	400	3	25
V773	ALL	1.85	1.98	1.73	0.06	(0.04)	455	475	440	7	25
UX Tau	ALL	8.72	9.23	8.28	0.29	(0.05)	440	455	425	9	25
BP Tau	ALL	92.57	103.49	88.63	4.50	(0.44)	480	500	450	13	30
	1	103.25	103.49	102.97	0.22		455	460	450	5	
	2	91.04	94.42	88.63	1.97		485	500	470	9	

flexure), a very similar morphology in the variance and surface difference plot are seen (lower panels Fig. 2). However, the variance profile remains lower than is observed. Also, the changes in EW due to these shifts are 0.04 Å, which is far below our estimated experimental error and the measured variations. To produce the same level of variations in the EW measurements, a drift rate of over six times the instrument flexure is needed. This suggests that though some of these variations could be due to instrument flexure, it is on the low level, and measured changes in the EW are unlikely to come from these instabilities.

As a result of these checks, the variations observed in the profiles are believed to be true variations in the emission from these objects.

4 ORIGIN OF Hα EMISSION

The most dominant known sources of Hα emission in YSOs are chromospheric activity and accretion. All the objects are likely candidates for accretion, as they are all thought to have circumstellar discs at sufficiently young ages. There is a number of ways to determine whether the emission is solely from chromospheric activity or not.

4.1 Hα measurements

The most common method to determine whether a stellar object is accreting or not is to use the Hα EW and 10 w measurements. The standard limits between an accreting and a non-accreting T Tauri star are EW of 10 Å and a 10 w of 270 km s^{-1} (White & Basri 2003). The limits in the EW come from the fact that these young stars are active and show some level of Hα emission from chromospheric activity alone. This activity is much weaker than the emission we expect from accretion especially in the case of T Tauri and Herbig Ae/Be stars (e.g. Manara et al. 2013). As chromospheric Hα emission depends strongly on spectral type, for the T Tauri stars in the sample, we use a spectral type dependent cut-off as given by Barrado y Navascués & Martín (2003).

The 10 w provides a measure of the broadening of the emission line. As the material in the accretion flows is free-falling to the stellar surface, it can reach velocities of 100s of km s^{-1}. These high velocities are then reflected in the broadening of the Hα line, and can be estimated by the 10 w of the emission line.

Using the EW cut-off based on spectral types by Barrado y Navascués & Martín (2003), and from Hα 10 w >270 km s^{-1}, we can classify all of our sample objects as accretors. The mean Hα EW and 10 w measurements for each object are given in Table 4.

For Herbig Ae objects, the chromospheric contribution to the Hα emission is likely to be very insignificant, as the emission decreases in earlier spectral types. In fact, it is more important to take consideration of the photospheric absorption in these objects. For example, in comparison to main-sequence objects of the same spectral type, Pickles (1998) give an absorption strength of 98 Å for A0, 93 Å for B1, 32 Å for F8, 25 Å for G2, and 0 Å for K5. This is quite significant compared to the emission measured in some of the early targets, and hence the EW measurements are underestimating the strength of the Hα emission in the sample. To account for this photospheric absorption, it is common to fit the observed spectrum with a main-sequence spectrum to estimate the photospheric contribution. Mendigutía et al. (2011a) removed the photospheric absorption in this way for a number of objects in this sample. For BF Ori, Mendigutía et al. (2011a) measured a mean EW of 9.9 Å compared to 3.8 Å here, for CO Ori they found 21.3 Å compared to 7.6 Å here and for RY Tau 15.3 Å compared to 10.4 Å in 2001 and 17.6 Å in 2003 here.

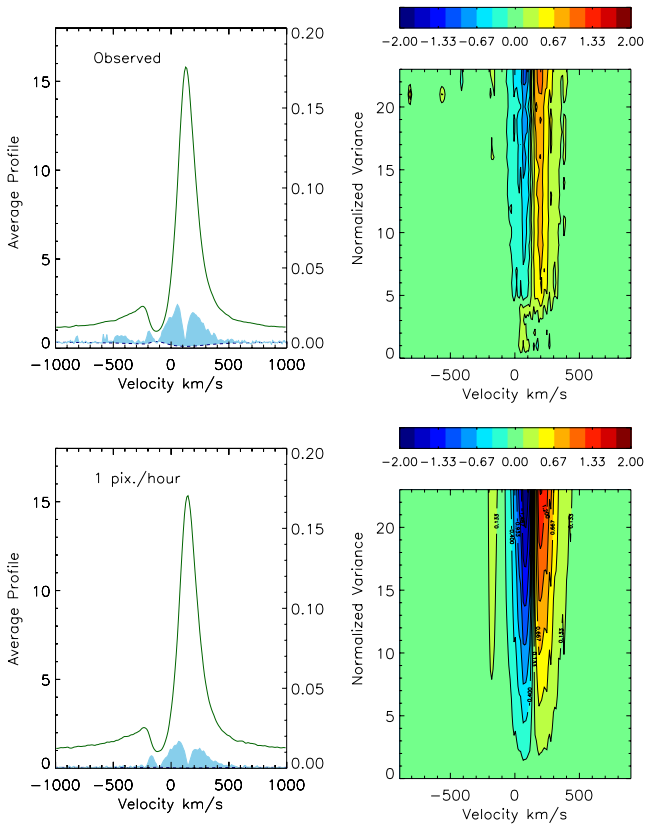

Figure 2. Top: observed variations in DR Tau in 2003. Bottom: taking the first spectrum of the 2003 DR Tau observations, a drift rate of 1 pixel shift h^{-1} was applied to simulate telescope flexure. This is equivalent to the instrument flexure, and results in a similar morphology in the variance profile and the surface plot as is observed. However, the EW variations remain an order of magnitude lower than what is observed.

This shows the removal of the absorption results in a significant difference for the weaker lines but not for the stronger emission lines. The EWs given in Table 4 are not corrected for photospheric absorption; however, before accretion rates are calculated a correction is applied. See Section 5 for further details.

4.2 Average and variance profiles

A typical characteristic of an accreting system is an asymmetric Hα emission line, often with more than one emission peak and overlying absorption features. Under the magnetospheric accretion model, the Hα emission originates in a structured flow of material. This results in emission across a large velocity range. Stellar winds and jets are associated with accreting systems (Ray et al. 2007), and can contribute both in the form of excess emission to the Hα line and overlying absorption features (see Section 4.4). This can be seen in many of Hα profiles in our sample. The average profiles for the sample show that the majority of the profiles are asymmetric, with many of them showing large absorption features.

Overplotted in blue on each average profile in the second row of Fig. 1 are the variance profiles for each object and each observation block. These profiles indicate clearly which parts of the profiles show the most changes. In most cases, where large changes occur they are confined to discrete wavelength ranges. This is also further evidence that there are multiple components within the emission lines and that it is not all from a single point, i.e. the central star.

4.3 Chromospheric activity versus accretion

There have been limited studies into the activity in accreting stars, mainly because both accretion and chromospheric activity cause similar emission in certain emission lines (Hα, Ca, He etc.) as well as UV and X-ray excess emission (Fuhrmeister et al. 2008; Curran et al. 2011). However, there has been some recent work on chromospheric activity by Manara et al. (2013), focusing on lower mass objects than in this sample.

Flares have distinct rise and decay profiles by comparison to accretion events, making this one of the most commonly used attributes to distinguish between the two events. So, if a rapid rise in EW occurs, followed by a slow decay, it is usually attributed to a flare. Guenther & Ball (1998) found accretion and flare events using spectroscopic monitoring of weak-lined T Tauri stars (WTTS) and classical T Tauri stars (CTTS). From ∼9500 spectra of CTTS, and 7200 of WTTS in Chamaeleon and Taurus they found 24 flares in WTTS and 15 in the CTTS. The largest flare was found in a WTTS. Whilst they claim that flare activity on T Tauri stars is more common than solar flares, these numbers show that these events do not occur very often in either CTTS or WTTS. Guenther & Ball (1998) also observed many slow variations in EW across a night's observation which they attribute to rotation, or variations in accretion rate.

One definitive attribute of flares is that the Hα emission associated with it is nearly entirely limited to the line centre with some extension in the wings up to $<$100 km s^{-1} (Worden, Schneeberger & Giampapa 1981a; Robinson, Cram & Giampapa 1990). This can be seen in the observations of the CTTS by Guenther & Ball (1998), where the flaring produces relatively small symmetric emission peaks (20 per cent above the continuum). In some cases, small asymmetries in the emission lines were seen, which are thought to be connected to coronal mass ejections . For Hα, this took the form of excess emission in the blue wing which moved through the line as the material is ejected from the atmosphere of the star. However, in the case of the WTTS IM Lupi, the authors argued that the asymmetries observed in the Hα profile are more likely to be associated with accretion activity rather than a flare (Günther et al. 2010).

In T Tauri stars, the range of time-scales for flare events is 10^2–10^4 s (Worden et al. 1981b). Although the sample does not have exhaustive time coverage, the rapid events do not show the typical fast rise and slow exponential decay expected of flares. Stellar flares can rise to a peak within a few minutes, while the decay can also happen within half an hour or so (Liefke, Fuhrmeister & Schmitt 2010), but it is much more usual to have flares lasting hours to days (Kuerster & Schmitt 1996; Schmitt & Favata 1999; Favata et al. 2000).

Finally, the strength of the Hα emission from accretion is much larger than emission from the majority of flares. Thus, it is expected that any change in accretion rate will have a much stronger effect on the emission line profile than any flare activity.

Thus, the variations and morphology of the emission seen in this sample, make it unlikely that the majority of the events are from chromospheric activity.

4.4 Emission from outflows

The traditional tracers of outflows and jets in YSOs are forbidden emission lines such as [O I] λ6300, 6363 Å, [N II] λ6583 Å, and [S II] λ6716, 6731 Å (Hartigan, Edwards & Ghandour 1995). However, it has also been shown using spectro-astrometry that these outflows can contribute to the Hα emission. This mostly takes the form of additional emission on the blue side, but cases have been

Table 5. Detections of other emission lines. [O I] λ6300 and λ6363 Å are associated with wind emission. The wavelength coverage is slightly smaller in the 2001 observations, so the [O I]λ6300 is not covered by these observations. No [S II] (λ6715, 6729 Å) or [N II] (λ6548.4, 6583.4 Å) emission were detected in any of the observations, are usually associated with stellar jets. The emission line He I λ 6678.2 Å which was detected in a number of targets, which is associated both with outflows and accretion.

Name	Year	[O I] λ6300 Å	[O I] λ6363 Å	He I λ6678.2 Å
RY Tau	2003	Yes	No	No
	2001	–	No	No
AB Aur	2003	Yes	Yes	Yes
	2001	–	Yes	Yes
T Tau	2003	Yes	No	No
	2001	–	No	No
SU Aur	2003	No	No	No
	2001	–	No	No
DR Tau	2003	Yes	Yes	Yes
	2001	–	Yes	Yes
RW Aur	2003	Yes	Yes	Yes
	2001	–	Yes	Yes
GW Ori	2003	Yes	Yes	No
	2001	–	No	No
V773 Tau	2003	Yes	No	No
UX Tau A	2003	Yes	No	No
BP Tau	2003	Yes	No	Yes
BF Ori	2001	–	Yes	No
LkHα 215	2001	–	No	No
MWC 480	2001	–	No	Yes
HD141569	2001	–	No	Yes
CO Ori	2001	–	No	Yes

found in which there is excess emission from the outflows found in both the blue and the red wings (Takami, Bailey & Chrysostomou 2003; Whelan, Ray & Bacciotti 2009).

Within the sample, signatures of [O I] λ6300 and 6363 Å were found in many of the targets (see Table 5), indicating that there is an outflow from these objects. In the majority of cases, the emission line was very narrow and weak (∼1 Å). This suggests that though there is probably some wind emission contaminating the Hα line, it is going to be a weak contribution.

Since the density of the outflowing material is much lower than the densities in the accretion flows, a small change in an accretion flow will produce the same change in emission as a large change in the outflow rate. This, along with the fact that the accretion emission will always be stronger in the Hα line than the outflow emission in an accreting object, makes it more likely that it is an accretion rate change. However, we cannot rule out that changes in the outflow have some contribution to the variations, so any accretion rate variations we derive are upper limits.

As a potential caveat, interferometric observations of the Herbig Be star, MWC 297 have found over 90 per cent of the Brγ emission to originate in a disc wind (Malbet et al. 2007). Furthermore, high-resolution spectra were taken, and modelling of the Brγ observed emission lead to the conclusion that the Brγ, Hα, and Hβ all formed in a disc wind, with the majority of the Hα and Hβ emission originating in the polar regions. Optical spectra were taken of MWC 297 from which an EW of 649 Å was found for Hα (Drew et al. 1997). Note that this is an order of magnitude higher than any Hα measured in this sample. Malbet et al. (2007) compared their wind model to these spectra and found the intensity of the Hα and Hβ lines to agree to within 10 per cent of observed intensities, and also found good agreement between the model line widths and those observed. Kraus et al. (2008) also found connections between Bγ emission and stellar wind in four out of five Herbig Ae/Be stars using interferometric data. In particular, they find the emitting area of the Brγ emission line to be correlated with the Hα profile. If a star shows an inverse P-Cygni profile, and a high accretion rate, the Brγ line is more likely to come from the accretion column, whereas if the Hα emission line is single or double peaked, Brγ is emitted in a greater area consistent with a disc or stellar wind. These interferometry results (Kraus et al. 2008) are in line with the earlier Hα spectro-polarimetry work of Vink et al. (2002), where it was found that the later Herbig Ae stars have a compact line-forming region, similar to that seen in T Tauri stars (Vink et al. 2003, 2005), whilst the earlier type Herbig Be stars have a larger line-forming region.

As this sample does not contain Herbig Be stars, it can be argued that it is not necessary to be overly concerned about disc winds providing the line emission in the sample. Moreover, recent studies of accretion diagnostics in Herbig Ae/Be stars (F0–O9) using the large wavelength coverage of X-Shooter (300–2500 nm) have also taken place. Pogodin et al. (2012) found that accretion rates derived from Hα to be in good agreement with accretion rates derived from indicators which can only originate in the high-temperature region close to the stellar surface. The variations in the Hα accretion rate were also found to follow the accretion rates from the other indicators, and showed a similar magnitude of variations. This is a strong suggestion that the changes in the Hα emission of Herbig Ae/Be stars follow the changes in accretion rate, or if Hα is indeed primarily a wind indicator for all these objects, then the wind emission is very closely connected to the accretion emission as suggested by magnetospheric accretion models.

Other studies have shown that, though there is a strong correlation between *U*-band excess and Hα luminosity, the variations in both do not follow each other in every case (Mendigutía et al. 2011b). Mendigutía et al. (2013) found a close agreement between the accretion rates derived from the Balmer excess and Hα emission in two Herbig Ae stars (one is also in this sample, MWC 480). Despite this agreement, they suggest the variations in the strength of the Hα emission to be uncorrelated to the variations in the Balmer excess. This is an indication that there is either a time delay in the variations in the emission lines that is not seen in the low-mass accretors, or the variations in the lines originate from some other process than accretion. Nonetheless, the level of the variations in these cases are low, so the correlation could be washed out by any noise in the observations. More sensitive observations are needed to confirm this.

Multiwavelength studies with X-shooter have also been undertaken with low-mass T Tauri stars (Rigliaco et al. 2012), which again find the Hα emission to be correlated with the UV excess and other indicators. There is substantial evidence confirming the effectiveness of using the Hα emission as an accretion rate estimator across the whole mass range of this sample, even if it is partially contaminated by wind emission.

4.5 Variations from continuum changes

Changes in the accretion rate will lead to changes in the veiling in the stellar continuum. This can lead to measured changes in the EW while the line emission remains steady. As the spectra in this work are not flux calibrated, changes in the continuum cannot be accounted for. The majority of the targets in this sample are optically variable (i.e. see Grankin et al. 2007 for light curves of eight targets), and so it can be expected that some changes in the continuum level occur over the course of these observations.

However, a change in the continuum will lead to a change in the emission across the whole line. This is not what is seen in this sample (i.e. see Fig. 1). The variance profiles attest to the fact that the variations measured originate in a narrow wavelength ranges within the profiles. This strongly suggests that even if there are continuum changes during the observations, they are not significant compared to those changes that occur within the profile emission.

It has been reported that continuum changes in these objects are also likely to come from occultations of the star by orbiting circumstellar clouds (Grinin et al. 1994; Mendigutía et al. 2011b). However, apart from some known exceptions (see Grinin et al. 1994), these occultations are expected to cause both a fall in the continuum and line emission.

4.6 Previous observations

The objects within the sample are mostly well-studied objects. Many of them have previous observations of other accretion-related emission lines, as well as confirmed accretion with UV excess measurements, which is considered to be the most direct indicator of ongoing accretion. These detections are discussed on an individual object basis in the Appendix.

The above arguments point towards accretion being the primary source of the emission observed and the variations in the emission lines. Through the following sections, it is assumed that the contribution of chromospheric and wind emission to the Hα line is negligible, and that any variations observed are the result of changes in the accretion rate.

5 ACCRETION RATES

Making the assumption that all of the Hα emission originates in accretion flows, we can calculate accretion rates from the Hα EW measurements for all objects in the sample.

5.1 Derivation of accretion luminosity relation

A number of relations have been derived between the Hα line luminosity and accretion luminosity (e.g. Herczeg & Hillenbrand 2008). Since the mass range of our sample lies in between those of the majority of these relations, we derived a new relation between Hα luminosity and accretion luminosity using the readily available data sets of Mendigutía et al. (2012) and Alcalá et al. (2014). The relation of Mendigutía et al. (2012) was derived using photospheric-corrected Hα emission (see Section 4.1) and quasi-simultaneous *U*-band photometry in a sample range of $\sim$1.5–5 $M_{\odot}$. Alcalá et al. (2014) derived accretion luminosities by fitting X-shooter spectra with a slab model, and used the Hα emission in the same spectra to derive Hα luminosities across a sample range of $\sim$0.03 to $\sim$1.2 $M_{\odot}$.

The accretion luminosities and Hα luminosities from both these samples are plotted in Fig. 3. A least-squares regression was applied to the combined sample, using the PYTHON procedure *stats.linregress* (*scipy* library), and the derived relations took the form of

$$\log(L_{\rm acc}) = {\rm A} + {\rm B} \cdot \log(L_{\rm H\alpha}), \quad (4)$$

where A = 3.14 ± 0.19 and B = 1.48 ± 0.06. This fit is shown as a solid black line in Fig. 3. The grey shaded region around this fit represents the 2σ confidence interval. The relation found here is similar to that found by Alcalá et al. (2014), where A = 1.50 ± 0.26 and B = 1.12 ± 0.07 (represented by a yellow dashed line in Fig. 3). Also, the relation found here is also very similar to that found by Herczeg & Hillenbrand (2008), where A = 2.0 ± 0.4 and B = 1.20 ± 0.11. However, the higher mass relation found by Mendigutía et al. (2012) is shallower, with A = 2.28 ± 0.25 and B = 1.09 ± 0.16, as indicated by the blue dashed line.

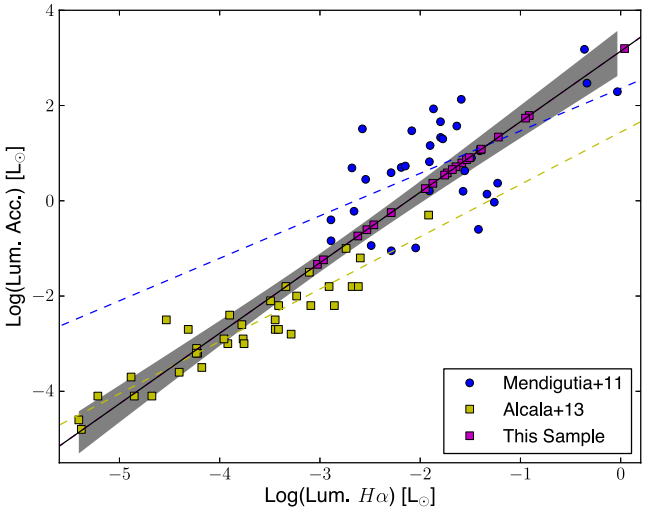

Figure 3. Accretion luminosity versus Hα line luminosity. Yellow points indicate those taken from Alcalá et al. (2014) and blue points from Mendigutía et al. (2011b). Yellow dashed line and blue dashed line represent the linear fits to these separate data sets. The solid black line indicates the fit to both data sets. The shaded grey region indicates the 2σ confidence interval around this fit. The purple data points in this plot represent the targets within this work, where 2003 and 2001 data are represented separately.

5.2 Derivation of accretion rates

Before deriving the accretion rates from the EW, they were corrected for photospheric absorption. This was done by adding the strength of the absorption in the nearest spectral type as given by Pickles (1998). The photospheric corrections used in each case are given in Table 6.

In order to convert an Hα EW to luminosity, it is first necessary to convert the EW to a flux. This was done by selecting the closest Kurucz model (Kurucz 1979) in spectral type and surface gravity to each of the sample members. (For some of the sample, surface gravities were not available so they were assumed; see Table 6). A line was fitted to the model continuum over the wavelength ranges 6450–6500 and 6620–6720 Å, and was used to find a continuum flux estimate at the line centre (6562.81 Å). Using these continuum estimates (given in Table 6), the EW can be transformed to a flux per unit area on the stellar surface (erg $s^{-1}cm^{-2}$), which is then converted to a luminosity ($L_{\rm H\alpha}$) using the published stellar radii given in Table 6. This step assumes that the source of the line luminosity is distributed uniformly across surface of the star. As the actual distribution of the accretion flow is unknown, this is commonly taken as a reasonable approximation.

Equation (4) is then used to determine accretion luminosities; however, the spread coefficients is not taken into account as they originate from the empirical derivation of this relation. Assuming that all the gravitational energy from the accretion is converted into luminosity, the accretion luminosity is related to the accretion rate ($\dot{M}$) as follows (Herczeg & Hillenbrand 2008):

$$\dot{M} = \left(1 - \frac{R_*}{R_{\rm in}}\right)^{-1} \cdot \frac{L_{\rm acc} R_*}{G M_*}. \quad (5)$$

Table 6. Parameters used in the derivation of accretion rates. The first column contains photospheric absorption correction taken from Pickles (1998). References for stellar masses and radii are given in Table. 2. For some objects in the sample, estimates of inner radii from observations were available. For the majority of the sample, an inner radius was assumed, similarly for surface gravity estimates. The continuum under the Hα line was estimated from the Kurucz (1993) stellar atmosphere models. Fluxes are in units of (ergs sec^{-1}cm^{-2} Å^{-1}).

Object	Phot. Hα EW (Å)	M_* ($M_\odot$)	R_* ($R_\odot$)	R_{in} (R_*)	log(g) (cm s^{-2})	F_{cont} (10^6)
RY Tau	1.3[a]	2.0	2.7	10[b]	4.2[e]	8.439
AB Aur	9.8	2.5	2.5	5[c]	4.1[f]	3.513
T Tau	1.3[a]	2.0	3.3	5[A]	4.1[g]	4.858
SU Aur	2.5	2.0	1.0	3[c, d]	3.9[h]	8.355
DR Tau	0.0	1.0	1.2	10[b]	2.8[g]	1.621
RW Aur	1.3[a]	1.0	2.7	5[A]	3.0[A]	3.026
GW Ori	1.9	3.7	2.5	3[c]	4.0[A]	8.439
BF Ori	9.8	2.5	1.3	3[A]	3.8[e]	2.796
LkHα 215	9.8	4.8	5.4	3[A]	4.0[A]	59.47
MWC 480	9.3	2.3	2.1	3[A]	3.5[i]	2.789
CO Ori	3.2	2.5	4.3	5[A]	3.1[e]	9.936
V773 Tau	0.6	1.2	2.4	5[A]	4.3[g]	4.853
UX Tau	0.6	1.3	2.7	5[A]	4.1[g]	4.858
BP Tau	0.0	0.8	7.6	5[A]	3.7[j]	1.615

[a]In the case of RY Tau, T Tau and RW Aur no K1 spectral type was available in catalogue so K0 was used in its place.
References: [A]Assumed (see Section 5 for more.), [b]Kitamura et al. (2002), [c]Vink et al. (2005), [d]Akeson et al. (2002), [e]Montesinos et al. (2009), [f]Bohm & Catala (1993), [g]Taguchi, Itoh & Mukai (2009), [h]DeWarf et al. (2003), [i]Hubrig et al. (2011), [j]Johns-Krull, Valenti & Koresko (1999).

Here, R_* is the stellar radius, R_{in} is the infall radius and M_* is the stellar mass. Gullbring et al. (1998) approximates the factor $(1 - \frac{R_*}{R_{in}})^{-1} \sim 1.25$, assuming $R_{in} \sim 5R_*$, which is appropriate for T Tauri stars. An infall radius of $R_{in} \sim 2.5R_*$ has been calculated to be more suitable for the higher rotation velocities in Herbig Ae stars (Muzerolle et al. 2004). Observations of inner-hole sizes were provided in the linear spectro-polarimetry study of Vink et al. (2005), these were used where possible, along with other published values. For the rest of the sample, an infall radius of $5R_*$ was assumed for the lower mass stars, and in keeping with observations of Herbig Ae stars, an infall radius of $3R_*$ was assumed for the higher mass objects. The assumed infall radii, continuum estimates from the models, and the published stellar mass and stellar radii used in the accretion calculations are all given in Table 6.

The mean accretion measurements for each object and for each night are given in Table 7. Also given, are error estimates, calculated by carrying the Hα EW estimated errors through the accretion relations.

Note, this relation (equation 4) was derived using the entire line emission. Therefore, it includes excess emission from wind and chromosphere, the effects of which will have been averaged out over the calibrating sample. The absolute value is then close to what would be measured from the UV excess, but the variations can still be affected by these extra sources of emission.

The mean accretion rate spread for a single night for Hα EW is 0.01–0.07 dex. Half of the sample have multiple nights observations so a measure of the spread in accretion rates from one night's observation to the next could be obtained. This inter night spread, 0.04–0.4 dex, is an order of magnitude larger than the spread on a single night. There are seven targets that have observations in both 2001 and 2003 (see Table 8), when comparing the accretion rates for these seven objects over the two years the spread is 0.13–0.52 dex.

5.3 Comparison with other accretion rate relations

The Hα 10 w can also be used to estimate the accretion rate. A relation for low-mass T Tauri and brown dwarfs was derived by Natta et al. (2004), and is useful in the cases where little or no stellar continuum can be detected. It has been proved to be a very good indicator of accretion (White & Basri 2003); however, as was shown in Costigan et al. (2012), its accuracy as a measurement of accretion has been called into question. As we showed in the sample of Costigan et al. (2012), the Hα 10 w had much larger variations than the two other accretion indicators, Hα EW and Ca II EW, demonstrating it is more likely to be affected by wind emission and line broadening processes than the freefall velocities within the accretion flow. Mendigutía et al. (2011a) show that in higher mass Herbig Ae/Be stars, the 10 w is strongly correlated with rotational velocities, and no correlation is found between the accretion rate and 10 w measurements. To test for this within our sample, the derived Hα EW derived accretion rate is plotted against the corresponding 10 w in Fig. 4. This plot again confirms that there is very little correlation between the two accretion indicators, and for this reason no accretion rates derived from the 10 w are discussed in this work.

6 DISCUSSION

This paper sets out to constrain the variations in the Hα emission of accreting stars. The aim here was to isolate the relative variability of the mass accretion rate as derived from the emission in each star. Thus, we do not take into account any systematic uncertainties from stellar parameters or line luminosity conversions (which will affect the comparison of the accretion values measured for different stars). Only the accuracy in our line measurements are considered in order to ascertain whether the observed variations we measure are above the measurement errors. Though some of the variations may come from sources other than accretion such as winds or from secondary accretion effects such as continuum changes (see Section 4), these measurements allow us to put an upper limit on the accretion rate changes as observed in the Hα emission line.

As previously mentioned, there are two distinct types of behaviour observed in this sample, slow variations and rapid events. In the following section, possible origins of each are discussed.

6.1 Slow variations: rotational modulation of the accretion rate

In the majority of the cases in this sample, small changes are seen in the profiles across the time-scale of our observation blocks. These variations are referred to as slow variations. These occur in discrete wavelength ranges, and take the form of a gradual change in the profile emission. These variations do not translate to large accretion rate changes and on average they result in changes of the accretion rate derived from Hα EW of 0.01–0.07 dex. When the changes between different nights of observations are examined in this sample, the spread in accretion rate variations increases slightly to 0.04–0.4 dex (see Table 7). Comparing the difference in derived accretion rates for the objects with observations in 2001 and 2003, this spread does not increase from the individual observation periods remaining at 0.13–0.52 dex. This is a strong indication that the time-scales of days are the dominant time-scales for these variations.

Table 7. Accretion rates derived from Hα EW. The average for all observations in 2001 and 2003 campaign is given, as well as the average for each observation block in the cases of multiple observations. Following each average is the (max–min) spread in accretion rates over the observation period. Units are $M_\odot$ yr^{-1}. Errors are calculated by carrying the Hα EW errors through the accretion rate calculation.

			2001								
2001	Log($\dot{M}$)		Night 1		Night 2		2.2		2.3		Error
	Av.	(Spread)	Av.	(Spread)	Av.	(Spread)	Av.	(Spread)	Av.	(Spread)	
RY Tau	−7.059	[0.024]									(0.004)
AB Aur	−5.604	[0.036]	−5.591	[0.008]	−5.603	[0.008]	−5.604	[0.009]	−5.620	[0.005]	(0.005)
T Tau	−5.851	[0.275]	−5.724	[0.005]	−5.936	[0.087]					(0.005)
SU Aur	−8.955	[0.135]	−9.016	[0.012]	−8.895	[0.016]					(0.007)
DR Tau	−8.111	[0.191]	−7.991	[0.010]	−8.148	[0.052]					(0.007)
RW Aur	−6.169	[0.112]									(0.031)
GW Ori	−6.945	[0.014]									(0.005)
BF Ori	−7.232	[0.035]									(0.005)
LkHα 215	−4.067	[0.014]									(0.004)
MWC 480	−6.274	[0.163]	−6.292	[0.040]	−6.314	[0.061]	−6.186	[0.012]	−6.308	[0.061]	(0.011)
CO Ori	−6.252	[0.041]									(0.006)

			2003								
2003	Log($\dot{M}$)		Night 1		Night 2		Night 3		Night 4		Error
	Av.	(Spread)	Av.	(Spread)	Av.	(Spread)	Av.	(Spread)	Av.	(Spread)	
RY Tau	−6.745	[0.302]	−6.573	[0.113]	−6.832	[0.012]	−6.796	[0.011]			(0.004)
AB Aur	−5.660	[0.111]	−5.610	[0.010]	−5.645	[0.006]	−5.661	[0.049]	−5.713	[0.004]	(0.004)
T Tau	−6.105	[0.020]									(0.005)
SU Aur	−8.880	[0.354]	−8.708	[0.033]	−8.981	[0.054]	−9.047	[0.035]			(0.007)
DR Tau	−7.973	[0.021]									(0.002)
RW Aur	−6.269	[0.410]	−6.439	[0.160]	−6.157	[0.031]					(0.032)
GW Ori	−6.622	[0.006]									(0.002)
V773 Tau	−7.663	[0.066]									(0.011)
UX Tau	−7.325	[0.065]									(0.003)
BP Tau	−6.166	[0.104]	−6.091	[0.003]	−6.177	[0.040]					(0.003)

Table 8. Comparison of accretion rates from 2003 to 2001 observations. Here, the averages for each year's observations are given, along with the spread [max–min]. Also given is the average over both periods and the spread in accretion rate estimates. Units are $M_\odot$ yr^{-1}.

Object	Log($\dot{M}$) 2001		Log($\dot{M}$) 2003		Both	
	Av.	(Spread)	Av.	(Spread)	Av.	(Spread)
RY Tau	−7.059	[0.024]	−6.745	[0.302]	−6.826	[0.519]
AB Aur	−5.604	[0.036]	−5.660	[0.111]	−5.632	[0.129]
SU Aur	−8.955	[0.135]	−8.880	[0.354]	−8.900	[0.354]
RW Aur	−6.169	[0.112]	−6.269	[0.410]	−6.248	[0.443]
DR Tau	−8.111	[0.191]	−7.973	[0.021]	−8.037	[0.212]
T Tau	−5.851	[0.275]	−6.105	[0.020]	−5.941	[0.391]
GW Ori	−6.945	[0.014]	−6.622	[0.006]	−6.710	[0.334]

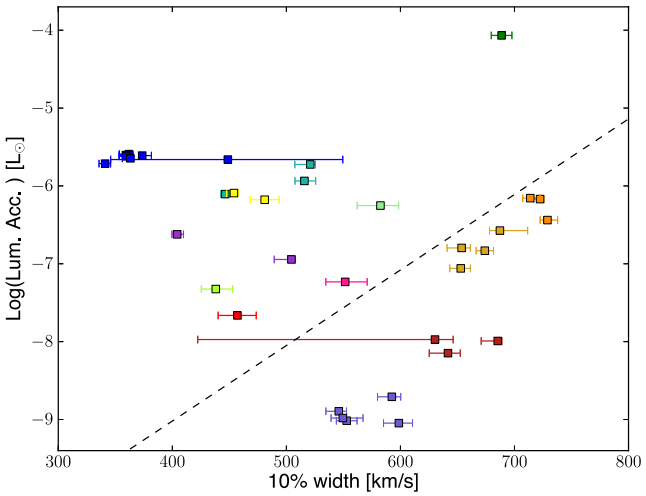

Figure 4. Average Hα EW derived accretion rate versus the average Hα 10 w. Error bars represent the max–min spread in each. Measurements for each observation block of each object are compared, and the colours represent different objects. The overplotted dashed line is the accretion rate to 10 w relation Log($M_{\rm acc}$) $\sim -12.9 + 0.0097 \cdot (10\,w)$ empirically derived by Natta et al. (2004) for brown dwarf and T Tauri objects. As found previously by Mendigutía et al. (2011a), this plot shows that the two measurements are not correlated in the higher mass regime.

Fig. 5 shows a comparison of accretion rate variations on all the time-scales in the sample. For each object, every accretion rate measurement is compared with every other accretion rate measurement for that object. In this way all the time-scales available in the sample can be exploited. The mean accretion rate is then plotted for each time bin for that object. In all cases but two, the variations reach a maximum after the first few days of observations. It shows that the dominant time-scale of variations in this sample is of the order of days. Two objects do show a rise in variations on the year time-scales, GW Ori and RY Tau. In the case of GW Ori, the sharp rise could be due to the lack of observations over consecutive days, and is probably not a real increase in accretion variations on the longer time-scales (see Fig. 5). For RY Tau, it could be a real rise in accretion variations, but it is more likely to be a single event observed at the end of the time series. (See Figs A17 and A18 for un-binned comparison of accretion variations and time-scales for all objects.)

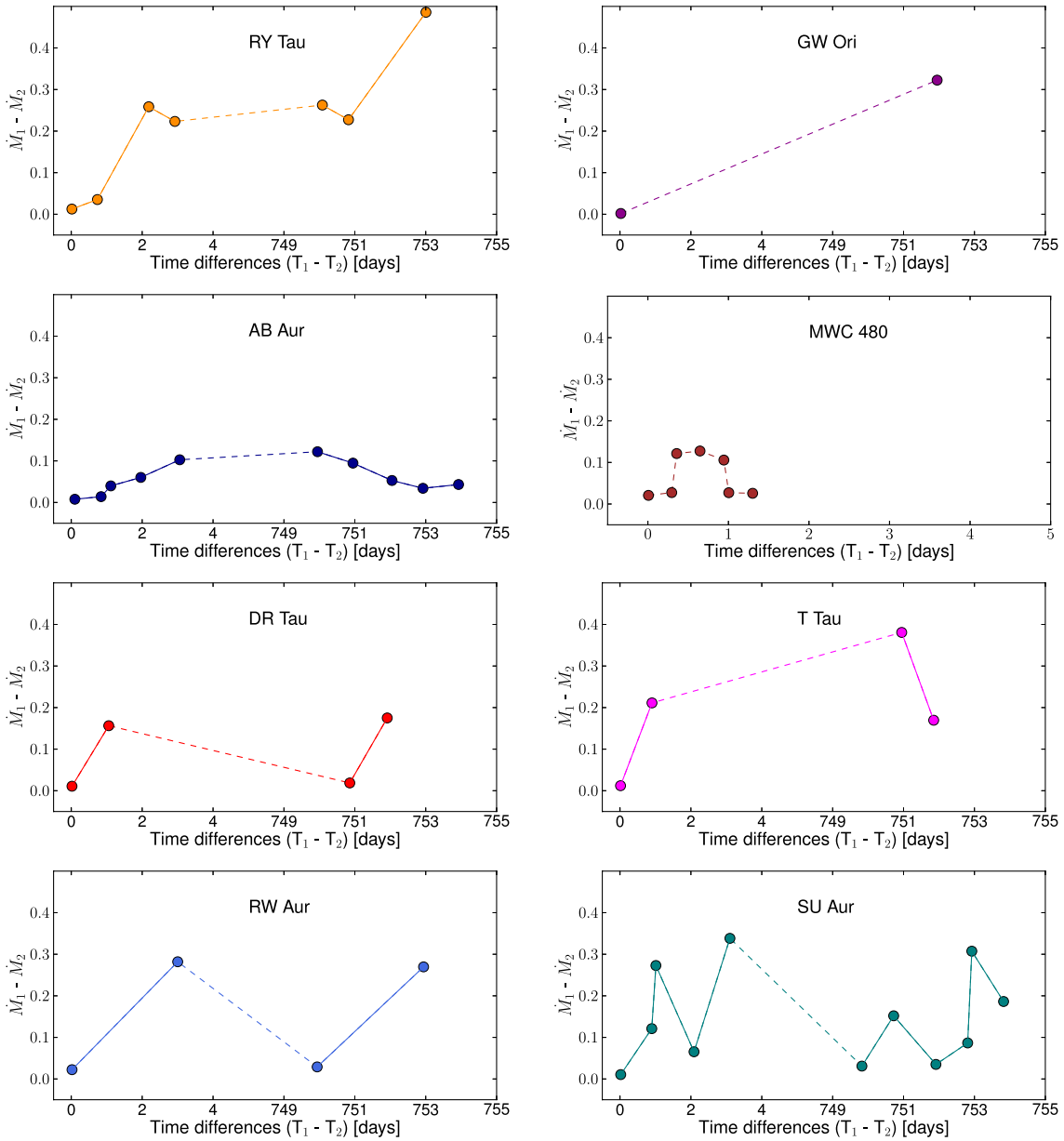

Figure 5. Mean differences in accretion rates [Log($M_\odot$ yr^{-1})] versus the time difference (d). In this case, we compare all accretion rates for each object, in order to cover all time-scales within the sample. The difference between all accretion rates was calculated, and the mean is plotted for each time bin. The time bins vary from object to object depending on the number of observations blocks. The same plot for all objects where the accretion rate differences are not binned can be seen in Figs A17 and A18.

The time-scales over which the accretion rate variations reach a maximum are comparable to the rotation periods within this sample, which all lie between ∼1 and 5 d (see Table 2). These slow variations in the profiles are consistent with what one would expect from a rotational modulation of the accretion rate. In the case of an asymmetric accretion flow, as the star rotates, different parts of the accretion flow will come into view, changing how much of the accretion flow is visible and what velocities within the flow are visible. Apart from three cases, no major changes are seen in the profiles within the single blocks of observations. These blocks represent time-scales of about an hour or less. In this sample, it appears that the small, gradual changes we see within these observation blocks accumulate to larger variations between the different nights of observations.

Our previous work on a sample of T Tauri stars in Chameleon supports this result. We monitored the Hα variations over time periods of weeks – 15 months, and also found that it was the short time-scales, of a few weeks or less, that were the dominant time-scales within the sample (Costigan et al. 2012). In Chameleon, we found the average spread in accretion rates to be 0.37 dex, which is very close to the variations we find in this sample of both T Tauri and Herbig Ae stars.

Simulations of magnetospheric accretion have found that even a slight offset (2°–5°) will result in an asymmetry in the accretion flow (Romanova et al. 2003). This is thought to be in the case for V2129 Oph (Alencar et al. 2012). The authors used magnetohydrodynamic (MHD) simulations of the observed magnetic octupole and dipolar fields of V2129 Oph, and radiative transfer codes to reproduce the

observed spectral line profiles. Earlier observations of the magnetic field found an offset between the octupole and dipole fields (15° and 25°) and the rotation axis (Donati et al. 2011). The modelling of these fields result in two ordered flows of material on to the star very close to the poles. The derived profile variations are similar in magnitude to the observed profiles, however the changes in the profile shape are not. At an inclination angle of 60° to the viewer, the models result in a change in 8 Å in Hα EW across the rotation period.

The changes that are observed in this sample over multiple days, are of the same order of magnitude as those modelled for V2129 Oph. For example AB Aur, RY Tau, SU Aur, BP Tau all have EW ranges of 5–15 Å between multiple nights observations. RW Aur has a much larger spread of 35 Å, which may mean that this model of two rotating flows is probably not sufficient to explain all of the variations seen in this object.

We can expect that rotationally induced apparent accretion rate change will depend on the inclination of the systems to our line of sight. Kurosawa, Harries & Symington (2006) showed through MHD simulations that as the inclination of an accreting system increases, the EW of the Hα emission decreases. This is due to the fact that we see less of the accretion flow at higher angles. In these models, as the inclination increases from 10° to 80° the EW changes from 32 Å to 21 Å. One can also expect to see more changes in the Hα EW if the system is inclined to our line of sight, making it more likely that the accretion flow will move in and out of view. In the 2003 observations, the three stars with the largest range in accretion rates in the sample are three of the most inclined systems. RY Tau, SU Aur, and RW Aur all have inclinations of 45° or over. DR Tau is also highly inclined, but does not show very large variations. However, since the system is close to edge on, we may not have a full view of the accretion flow, and the disc may obscure a lot of the light coming from the accretion flows. The inclination angles are given in Table 2.

This assertion no longer holds true when the 2001 observations are considered. The three objects (RY Tau, SU Aur, and RW Aur) show much less variability than the other objects, whereas DR Tau shows some of the largest accretion rate variations, and T Tau and MWC 480 with disc inclinations of ∼30° also show large variations. This suggests that a picture of a stable rotating asymmetric flow is probably too simplistic to describe the full variations in these objects.

Long-term photometric monitoring of accreting objects also support the scenario of a more complicated accretion flow as irregular light curves have been observed in many accreting T Tauri stars (Herbst et al. 1994; Scholz & Eislöffel 2004; Grankin et al. 2007; Scholz et al. 2009). Over the time-scales of years multiple different types of variations can been seen in one object. In many of the cases were variations occur on the time-scales of days, the simple explanation of a rotational modulation cannot explain the full behaviour.

In their spectro-polarimetric observations of BP Tau, Donati et al. (2008) found strong signatures of rotational modulation in the accretion related emission lines. The narrow emission lines associated with accretion (He I, Fe II, and narrow component of Ca II IR triplet) varied strongly with rotation period. However, the broad emission lines Hα, Hβ (and also the broad component of the Ca II IR triplet) were found to vary on the level of 10–20 per cent with rotation, with the remainder of the variations coming from seemingly other sources. This could be explained by the narrow emission component originating close to the base of the accretion flow, with the Hα emission originating in the bulk of the accretion flow, which may be more sensitive to instabilities. Excess contributions in the Hα emission from outflows could also play a role. The authors also suggest that changes in the rotational modulation of the longitudinal magnetic field between the two observation periods in 2006 February and December implies that the large-scale field topology was distorted by variability in the system between the two periods. This suggests though rotational modulation accounts for the majority of the variations, there are other ongoing processes.

There are many kinds of instabilities that can occur in the disc and accretion flow that may account for the changes in the variations observed over time, e.g. the buildup of material in the circumstellar disc (D'Angelo & Spruit 2012). Kurosawa & Romanova (2013) show that in the case where Rayleigh–Taylor instabilities exist in the inner disc, unstable accretion flows can form. These flows change in size, shape, and numbers, meaning there is always a accretion column visible. This results in a constantly observed red-shifted absorption in the Balmer lines, more particularly in the higher Balmer lines such as Hγ and Hδ. This has been observed in RW Aur (Edwards et al. 1994), where spectroscopic monitoring also confirmed the presence of an asymmetric accretion flow (Petrov et al. 2001), as well as for SU Aur (Johns & Basri 1995b; Petrov et al. 1996).

It is possible that these instabilities exist in some if not all of the objects in this sample. Comparing the 2001 and the 2003 sample, some changes are seen in the Hα profiles, but also differences in the derived accretion rates and their variations. These instabilities could account for changes in the Hα emission if they change the form of the accretion flows.

6.2 Rapid events

The rapid events observed in this sample do not fit into the frame of rotational modulation. AB Aur, and to a lesser extent RY Tau and RW Aur, show significant variations in the profile over the time-scale of 1 h. In the case of each star, these changes only occur during a single night of observations (for AB Aur see Fig. 6). A number of short-term rapid variations have previously been discovered in objects in our sample and these are presented in the following paragraphs.

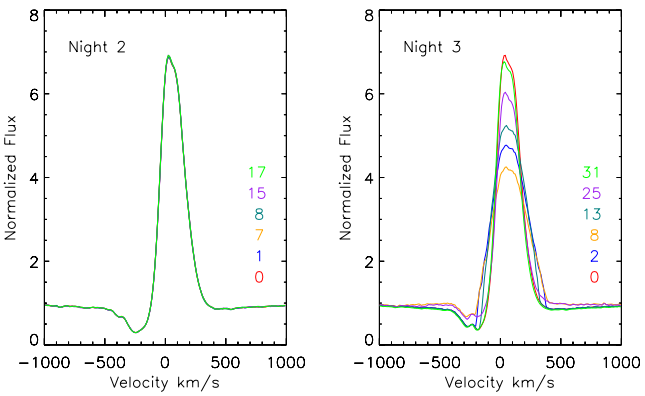

Figure 6. A comparison between a sub-set of profiles on two separate nights of the 2003 observations for AB AUR. On the second night of observations in 2003, no significant change within the profile was observed. The minute of the hour in which the spectrum was observed is given to the right of the profiles in the corresponding colour. During the third night of observations there were large changes. Shown here is a sequence of spectra where the emission line falls in strength, and broadens, before returning to the initial strength.

Short-term striking variations have been observed in the Hα profile of AB Aur previously, where changes occurred in both the intensity and profile shape. Beskrovnaya et al. (1995) described the changes as occurring during each observing night across the emission line but especially in the absorption feature of the P-Cygni profile and the emission peak. They attribute these variations to the motion of circumstellar inhomogeneities. This is similar to the changes observed in the Hα profile of AB Aur on night 3, where it oscillates between broad wings and low emission, and strong emission and with narrow wings. However, in the case of Beskrovnaya et al. (1995), their observations take place with hour separations, so they do not have the short-term cadence that we have in this sample.

Rapid variations have been seen in the Hγ profile of RW Aur, occurring on time-scales as short as 10 min. Over the course of the observations, the central absorption component of the Hγ line increased in EW by a factor of 2 within an hour (Mundt & Giampapa 1982). These variations were not reflected in the Hα emission, which is thought to be a result of the high optical thickness in the surrounding envelope. Mundt & Giampapa (1982) found these variations to be consistent with both flaring and accretion events.

Variations in Hα profile of RY Tau were found on the time-scales of 10–20 min without variations in the star's brightness (Kolotilov & Zajtseva 1975). Three separate nights observations took place covering time-scales of a few hours each night. The profiles changed between nights, but in two out of three occasions they were stable throughout the night. The brightness of the star was lower on the night of the variations than on the other two nights, which is an indication that these variations came from magnetic activity (Gullbring, Barwig & Schmitt 1997).

With the short wavelength coverage in this sample and no simultaneous alternative observations, the behaviour seen in AB Aur, RY Tau, or RW Aur cannot be properly defined, and the origin of these rapid variations is not clear. Gullbring (1994) argue that in the case of magnetospheric accretion short-term variability is to be expected. The in-fall time-scale of gas towards the pole is less than one hour. Any instabilities that occur in the disc or the magnetic field at the point of their interaction will lead to a clumpy flow of material on to the surface.

The changes in RY Tau and RW Aur take the form of a drop in emission across both lines, but not within the line centre, which would be more indicative of a flare (see Section 4.3). However, it is probable that the rapid events that are observed in RW Aur and RY Tau are due to a flare event. This is not the case with AB Aur. The rapid variations that occur in the profile of AB AUR are unique in the sample. In no other object do we see these changes in emission line strength, width and surrounding absorption.

It is possible that all the targets have these periods of rapid variations. Out of the total 22.6 h of observations, these rapid events only take place with three observation blocks, which constitutes 2.4 h or $\sim$10 per cent of our total observing time. This suggests they are not very common events and it rules out stochastic processes as the primary source of variations within the sample. However, these stochastic events could be the cause of the rapid variations we see in a small number and probably take the form of instabilities in the magnetic field (Goodson, Böhm & Winglee 1998), or inner disc (Kurosawa & Romanova 2013).

6.3 Comparison between Herbig Ae and T Tauri sample

Herbig Ae stars are the intermediate mass equivalent of T Tauri stars and are thought to go through a similar process of accretion as T Tauri stars. As they are higher mass, they are shorter lived, but retain their circumstellar disc for long enough to accrete material from them on to their surfaces.

Similar scalings of accretion rate to disc mass exist between T Tauri and Herbig Ae (Mendigutía et al. 2012). They also show that the near-infrared colour excess trend is the same across the T Tauri to Herbig Ae mass range, which can be explained by the reprocessing of both the stellar and accretion luminosities by the inner disc.

However, there is inconclusive evidence whether Herbig Ae stars are host to strong magnetic fields. Under our current understanding of magnetospheric accretion these strong, stable fields are essential for maintaining a quasi-stable accretion flow.

Within this work, a large mass range is covered (up to $\sim$5 $M_{\odot}$) and similar variations are seen in all objects. One of the larger mass targets, MWC 480 shows an accretion rate spread of 0.012–0.061 over single observation blocks. Comparing to one of the smallest mass targets in the sample, DR Tau with 0.010–0.052, shows there is little difference between the two. Indeed, others have found similar accretion rate variations for Herbig Ae stars as is found in this work, and the LAMP sample. For example Pogodin et al. (2012) observed accretion variations of amplitude 0.4 dex over the time-scales of 10 d for one target, while multiple targets showed variations of 0.3 dex between consecutive days observations. From 38 Herbig Ae/Be stars, Mendigutía et al. (2011b) found a typical upper limit of accretion variations of 0.5 dex over time-scales from days to months.

Compiling the samples from both studies (this and the LAMP sample), of 10 low-mass T Tauri and 14 intermediate-mass T Tauri/Herbig Ae stars, suggests that it is the same process that produces the Hα variations in T Tauri and Herbig Ae stars, across the entire mass range up to $\sim$5 $M_{\odot}$. This variability result is entirely consistent with earlier spectro-polarimetry surveys (Vink et al. 2002, 2003, 2005)

7 SUMMARY

This study was undertaken to put a lower limit on the time-scales of accretion variability in T Tauri and Herbig Ae stars. Our previous work, Costigan et al. (2012), used the Hα emission in low-mass T Tauri stars as a proxy for accretion, through which an upper limit of 8–25 d for the time-scales of accretion variations was found. These were the shortest time-scales in that sample.

This data set gave us the opportunity to approach the problem from the other end of the scale, by studying the variations on the time-scales of minutes, hours, days, and in a few cases years. The main findings of this work can be summarized as follows.

(i) The majority of variations observed in this sample take the form of slow variations, where gradual changes in the Hα emission occur across the $\sim$1 h observation blocks. These slow variations are consistent with what we would expect from accretion rate changes rather than solely chromospheric activity or wind emission.

(ii) Calculating the mass accretion rate from the Hα emission, the average spread the accretion rate on time-scales of less $\lesssim$1 h is found to be 0.01–0.07 dex. The spread increases by an order of magnitude when different nights' observations are considered, 0.04–0.4 dex. However, when the variations are considered over two years, they have not increased and remain the same, 0.13–0.52 dex.

(iii) Therefore, it is the period of days that is the dominant time-scales of these slow variations. These results are found to be consistent with a rotational modulation of the accretion rate and are supported by previous results.

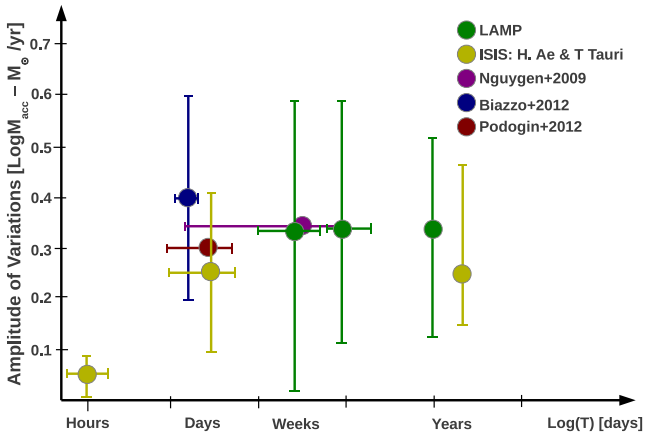

Figure 7. Amplitudes of accretion rate variations versus the time-scales over which they occur. Error bars here indicate the spread in accretion rates, and time coverage in each bin. Data from: Nguyen et al. (2009); Biazzo et al. (2012); Pogodin et al. (2012); Costigan et al. (2012) (LAMP).

(iv) Rapid events occur in three observation blocks, which constitute 2.4 h or ∼10 per cent of our total observing time. These events consist of fast changes within the Hα emission line on time-scales of less than an hour. They could be connected to instabilities in the magnetic field or inner disc, which would create more stochastic accretion events than we observe in the majority of the sample.

(v) This data set covers a large range in masses, in which very similar variations and accretion rate changes are found. This strongly suggests that the same process is taking place across the full mass range, from low-mass T Tauri stars up to Herbig Ae stars, and that the same model of accretion holds over large stellar mass range.

The dominant time-scales of the variations found in this data agree with those found in other studies. Fig. 7 is a graphical comparison of accretion variations found in different samples. The error bars within the plot, represent the parameter space covered by each data set, not the errors. This is not a complete sample of variability studies, but as these studies used similar accretion indicators, they are more comparable. For example, Pogodin et al. (2012) used a number of emission lines associated with accretion to estimate accretion rates in eight Herbig Ae stars. For half the sample, they have multiple observations covering time-scales of tens of days. By averaging across the accretion indicators, including Hα they found variations of 0.1–0.4 dex for these four objects. Biazzo et al. (2012), with a sample of 12 objects, found variations of 0.2–0.6 dex over the two days separating observations. The last data set in this comparison was covered by Nguyen et al. (2009), who found variations from Ca II emission of 0.35 dex on average over time-scales of days to months.

Through these studies, it has become clear that typical accretors do not go through large accretion bursts like EX Ors or even FU Ors (Herbig 1977, 2007). Over the time-scales of days, months and years, no large variations in accretion rate were found.

This work cannot rule out that large changes in the accretion could occur on time-scales of approximately decades or longer (as is the case with FU Ori). However, it can be said that over the time-scales of years, the dominant variations occur on time-scales close to the rotation period. This suggests that observations over the time-scale of < 1 week in typical accreting objects are sufficient to put limits on the expected magnitudes of variations that occur over the time-scales of years.

These low levels of variations are also significant for the $\dot{M}$–M_*^2 relation (see Mohanty et al. (2005)). The mean amplitude of variations in the samples studied here is ∼0.5 dex. This demonstrates that the ∼2 orders of magnitude scatter around the $\dot{M}$–M_*^2 relation at a given mass cannot be solely due to accretion variability. Studies of individual star-forming regions with low-age spreads have shown that this spread is unlikely to be due to evolutionary effects (i.e. Natta, Testi & Randich 2006). This strongly suggests that the $\dot{M}$–M_* relation is due to either limitations in our detections of low accretion rates in high-mass objects (Clarke & Pringle 2006; Barentsen et al. 2011), initial conditions (Alexander & Armitage 2006; Dullemond, Natta & Testi 2006) or is an indirect correlation where both the accretion rate and stellar mass are linked through a different process.

ACKNOWLEDGEMENTS

JSV would like to thank the UK Science and Technologies Facility Council (STFC) and the Northern Ireland Department of Culture Arts and Leisure (DCAL) for financial support. AS and TR would like to thank the Science Foundation of Ireland (SFI) for their support under grant numbers 11/RFP/AST/3331 and 10/RFP/AST2780.

REFERENCES

Akeson R. L., Ciardi D. R., van Belle G. T., Creech-Eakman M. J., 2002, ApJ, 566, 1124
Akeson R. L., Ciardi D., van Belle G. T., 2003, in Traub W. A., ed., Proc. SPIE Conf. Ser. Vol. 4838, Interferometry for Optical Astronomy II. SPIE, Bellingham, p. 1037
Alcalá J. M. et al., 2014, A&A, 561, A2
Alecian E., Peralta R., Oksala M. E., Neiner C., 2012, in Boissier S., de Laverny P., Nardetto N., Samadi R., Valls-Gabaud D., Wozniak H., eds, SF2A-2012: Proc. Annual meeting of the French Society of Astronomy and Astrophysics,The Magnetism in Massive Stars (MiMeS) Project: First HARPSpol Discoveries, p. 401
Alencar S. H. P. et al., 2012, A&A, 541, A116
Alexander R. D., Armitage P. J., 2006, ApJ, 639, L83
Baraffe I., Chabrier G., Gallardo J., 2009, ApJ, 702, L27
Barentsen G. et al., 2011, MNRAS, 415, 103
Barrado y Navascués D., Martín E. L., 2003, AJ, 126, 2997
Basri G., Bertout C., 1989, ApJ, 341, 340
Bertout C., Basri G., Bouvier J., 1988, ApJ, 330, 350
Beskrovnaya N. G., Pogodin M. A., Najdenov I. D., Romanyuk I. I., 1995, A&A, 298, 585
Biazzo K., Alcalá J. M., Covino E., Frasca A., Getman F., Spezzi L., 2012, A&A, 547, A104
Boden A. F. et al., 2007, ApJ, 670, 1214
Bohm T., Catala C., 1993, A&AS, 101, 629
Bouvier J., Bertout C., 1989, A&A, 211, 99
Bouvier J., Bertout C., Benz W., Mayor M., 1986, A&A, 165, 110
Bouvier J. et al., 2003, A&A, 409, 169
Calvet N., Muzerolle J., Briceño C., Hernández J., Hartmann L., Saucedo J. L., Gordon K. D., 2004, AJ, 128, 1294
Catala C. et al., 1999, A&A, 345, 884
Clarke C. J., Pringle J. E., 2006, MNRAS, 370, L10
Cody A. M., Tayar J., Hillenbrand L. A., Matthews J. M., Kallinger T., 2013, AJ, 145, 79
Cohen M., Kuhi L. V., 1979, ApJS, 41, 743
Costigan G., Scholz A., Stelzer B., Ray T., Vink J. S., Mohanty S., 2012, MNRAS, 427, 1344
Curran R. L., Argiroffi C., Sacco G. G., Orlando S., Peres G., Reale F., Maggio A., 2011, A&A, 526, A104
D'Angelo C. R., Spruit H. C., 2012, MNRAS, 420, 416

Davies J. K., Evans A., Bode M. F., Whittet D. C. B., 1990, MNRAS, 247, 517
de Winter D., van den Ancker M. E., Maira A., Thé P. S., Djie H. R. E. T. A., Redondo I., Eiroa C., Molster F. J., 2001, A&A, 380, 609
DeWarf L. E., Sepinsky J. F., Guinan E. F., Ribas I., Nadalin I., 2003, ApJ, 590, 357
Donati J.-F. et al, 2008, MNRAS, 386, 1234
Donati J.-F. et al., 2011, MNRAS, 412, 2454
Drew J. E., Busfield G., Hoare M. G., Murdoch K. A., Nixon C. A., Oudmaijer R. D., 1997, MNRAS, 286, 538
Dullemond C. P., Natta A., Testi L., 2006, ApJ, 645, L69
Dupree A. K. et al., 2012, ApJ, 750, 73
Edwards S., Hartigan P., Ghandour L., Andrulis C., 1994, AJ, 108, 1056
Eisner J. A., Lane B. F., Hillenbrand L. A., Akeson R. L., Sargent A. I., 2004, ApJ, 613, 1049
Espaillat C., Calvet N., D'Alessio P., Hernández J., Qi C., Hartmann L., Furlan E., Watson D. M., 2007, ApJ, 670, L135
Favata F., Reale F., Micela G., Sciortino S., Maggio A., Matsumoto H., 2000, A&A, 353, 987
Fuhrmeister B., Liefke C., Schmitt J. H. M. M., Reiners A., 2008, A&A, 487, 293
Fukagawa M. et al., 2004, ApJ, 605, L53
Garcia Lopez R., Natta A., Testi L., Habart E., 2006, A&A, 459, 837
Goodson A. P., Böhm K. H., Winglee R. M., 1998, in Holt S. S., Kallman T. R., eds, AIP Conf. Proc. Vol. 431, Accretion Processes in Astrophysical Systems: Some Like it Hot! Am. Inst. Phys., New York, p. 533
Grankin K. N., Melnikov S. Y., Bouvier J., Herbst W., Shevchenko V. S., 2007, A&A, 461, 183
Grankin K. N., Bouvier J., Herbst W., Melnikov S. Y., 2008, A&A, 479, 827
Grinin V. P., The P. S., de Winter D., Giampapa M., Rostopchina A. N., Tambovtseva L. V., van den Ancker M. E., 1994, A&A, 292, 165
Guenther E., Ball M., 1998, in Donahue R. A., Bookbinder J. A., eds, ASP Conf. Ser. Vol. 154, The Tenth Cambridge Workshop on Cool Stars, Stellar Systems and the Sun. Astron. Soc. Pac., San Francisco, p. 1701
Gullbring E., 1994, A&A, 287, 131
Gullbring E., Barwig H., Schmitt J. H. M. M., 1997, A&A, 324, 155
Gullbring E., Hartmann L., Briceno C., Calvet N., 1998, ApJ, 492, 323
Günther H. M., Matt S. P., Schmitt J. H. M. M., Güdel M., Li Z.-Y., Burton D. M., 2010, A&A, 519, A97
Hartigan P., Edwards S., Ghandour L., 1995, ApJ, 452, 736
Hartmann L., Hewett R., Stahler S., Mathieu R. D., 1986, ApJ, 309, 275
Herbig G. H., 1977, ApJ, 217, 693
Herbig G. H., 2007, AJ, 133, 2679
Herbig G. H., Bell K. R., 1988, Third Catalog of Emission-Line Stars of the Orion Population. Lick Observatory, Santa Cruz, CA
Herbst W., Layden A. C., 1987, AJ, 94, 150
Herbst W., Herbst D. K., Grossman E. J., Weinstein D., 1994, AJ, 108, 1906
Herbst W., Eislöffel J., Mundt R., Scholz A., 2007, Protostars and Planets V. Univ. Arizona Press, Tucson, AZ
Herczeg G. J., Hillenbrand L. A., 2008, ApJ, 681, 594
Hernández J., Calvet N., Briceño C., Hartmann L., Berlind P., 2004, AJ, 127, 1682
Hillenbrand L. A., Strom S. E., Vrba F. J., Keene J., 1992, ApJ, 397, 613
Hubrig S., Schöller M., Yudin R. V., 2004, A&A, 428, L1
Hubrig S. et al., 2011, A&A, 536, A45
Høg E. et al., 2000, A&A, 355, L27
Jaschek M., Jaschek C., Andrillat Y., 1988, A&AS, 72, 505
Johns C. M., Basri G., 1995a, AJ, 109, 2800
Johns C. M., Basri G., 1995b, ApJ, 449, 341
Johns-Krull C. M., Valenti J. A., Koresko C., 1999, ApJ, 516, 900
Kenyon S. J., Hartmann L., 1995, ApJS, 101, 117
Kitamura Y., Momose M., Yokogawa S., Kawabe R., Tamura M., Ida S., 2002, ApJ, 581, 357
Kolotilov E. A., Zajtseva G. V., 1975, Perem. Zvezdy, 20, 153
Königl A., 1991, ApJ, 370, L39
Kraus A. L., Hillenbrand L. A., 2009, ApJ, 704, 531
Kraus S. et al., 2008, A&A, 489, 1157
Kuerster M., Schmitt J. H. M. M., 1996, A&A, 311, 211
Kurosawa R., Romanova M. M., 2013, MNRAS, 431, 2673
Kurosawa R., Harries T. J., Symington N. H., 2006, MNRAS, 370, 580
Kurucz R. L., 1979, ApJS, 40, 1
Kurucz R. L., 1993, VizieR Online Data Catalog, 6039, 0
Liefke C., Fuhrmeister B., Schmitt J. H. M. M., 2010, A&A, 514, A94
López-Martín L., Cabrit S., Dougados C., 2003, A&A, 405, L1
Malbet F. et al., 2007, A&A, 464, 43
Manara C. F. et al., 2013, A&A, 551, A107
Mannings V., Sargent A. I., 1997, ApJ, 490, 792
Manoj P., Bhatt H. C., Maheswar G., Muneer S., 2006, ApJ, 653, 657
Mathieu R. D., Adams F. C., Latham D. W., 1991, AJ, 101, 2184
Mendigutía I., Eiroa C., Montesinos B., Mora A., Oudmaijer R. D., Merín B., Meeus G., 2011a, A&A, 529, A34
Mendigutía I., Calvet N., Montesinos B., Mora A., Muzerolle J., Eiroa C., Oudmaijer R. D., Merín B., 2011b, A&A, 535, A99
Mendigutía I., Mora A., Montesinos B., Eiroa C., Meeus G., Merín B., Oudmaijer R. D., 2012, A&A, 543, A59
Mendigutía I. et al., 2013, ApJ, 776, 44
Mohanty S., Jayawardhana R., Basri G., 2005, ApJ, 626, 498
Montesinos B., Eiroa C., Mora A., Merín B., 2009, A&A, 495, 901
Mora A. et al., 2001, A&A, 378, 116
Mundt R., Giampapa M. S., 1982, ApJ, 256, 156
Muzerolle J., D'Alessio P., Calvet N., Hartmann L., 2004, ApJ, 617, 406
Muzerolle J., Luhman K. L., Briceño C., Hartmann L., Calvet N., 2005, ApJ, 625, 906
Natta A., Prusti T., Neri R., Wooden D., Grinin V. P., Mannings V., 2001, A&A, 371, 186
Natta A., Testi L., Muzerolle J., Randich S., Comerón F., Persi P., 2004, A&A, 424, 603
Natta A., Testi L., Randich S., 2006, A&A, 452, 245
Nguyen D. C., Scholz A., van Kerkwijk M. H., Jayawardhana R., Brandeker A., 2009, ApJ, 694, L153
Petrov P. P., Gullbring E., Ilyin I., Gahm G. F., Tuominen I., Hackman T., Loden K., 1996, A&A, 314, 821
Petrov P. P., Gahm G. F., Gameiro J. F., Duemmler R., Ilyin I. V., Laakkonen T., Lago M. T. V. T., Tuominen I., 2001, A&A, 369, 993
Pickles A. J., 1998, PASP, 110, 863
Pogodin M. A., Hubrig S., Yudin R. V., Schöller M., González J. F., Stelzer B., 2012, Astron. Nachr., 333, 594
Praderie F., Catala C., Simon T., Boesgaard A. M., 1986, ApJ, 303, 311
Ray T., Dougados C., Bacciotti F., Eislöffel J., Chrysostomou A., 2007, in Reipurth V. B., Jewitt D., Keil K., eds, Protostars and Planets V. Univ. Arizona Press, Tucson, AZ, p. 231
Rigliaco E., Natta A., Testi L., Randich S., Alcalà J. M., Covino E., Stelzer B., 2012, A&A, 548, A56
Robinson R. D., Cram L. E., Giampapa M. S., 1990, ApJS, 74, 891
Romanova M. M., Ustyugova G. V., Koldoba A. V., Wick J. V., Lovelace R. V. E., 2003, ApJ, 595, 1009
Rydgren A. E., Vrba F. J., 1983, ApJ, 267, 191
Rydgren A. E., Strom S. E., Strom K. M., 1976, ApJS, 30, 307
Schmitt J. H. M. M., Favata F., 1999, Nature, 401, 44
Scholz A., Eislöffel J., 2004, A&A, 419, 249
Scholz A., Jayawardhana R., 2006, ApJ, 638, 1056
Scholz A., Xu X., Jayawardhana R., Wood K., Eislöffel J., Quinn C., 2009, MNRAS, 398, 873
Simon M., Dutrey A., Guilloteau S., 2000, ApJ, 545, 1034
Stelzer B., Scholz A., Jayawardhana R., 2007, ApJ, 671, 842
Taguchi Y., Itoh Y., Mukai T., 2009, PASJ, 61, 251
Takami M., Bailey J., Chrysostomou A., 2003, A&A, 397, 675
Vink J. S., Drew J. E., Harries T. J., Oudmaijer R. D., 2002, MNRAS, 337, 356
Vink J. S., Drew J. E., Harries T. J., Oudmaijer R. D., Unruh Y. C., 2003, A&A, 406, 703
Vink J. S., Drew J. E., Harries T. J., Oudmaijer R. D., Unruh Y., 2005, MNRAS, 359, 1049
Vrba F. J., Rydgren A. E., Zak D. S., Chugainov P. F., Shakhovskaya N. I., 1984, Bull. Am. Astron. Soc., 16, 998
Wade G. A. et al., 2005, A&A, 442, L31

Welty A. D., 1995, AJ, 110, 776
Whelan E. T., Ray T. P., Bacciotti F., 2009, ApJ, 691, L106
White R. J., Basri G., 2003, ApJ, 582, 1109
White R. J., Ghez A. M., 2001, ApJ, 556, 265
Worden S. P., Schneeberger T. J., Giampapa M. S., 1981a, ApJS, 46, 159
Worden S. P., Schneeberger T. J., Kuhn J. R., Africano J. L., 1981b, ApJ, 244, 520

APPENDIX A: DESCRIPTION

The properties of the individual targets used in the analysis in this paper are presented along with time series of the Hα profiles, average and variance profiles and differential surface and spectra plots (as given for AB Aur in Fig. 1). The appendix is included as online material.

Also within the appendix are plots for each object showing the difference between two accretion rate measurements [Log($M_\odot$ yr^{-1})] versus their time difference (d). These are similar to Fig. 5; however, in this case, the accretion rate differences in each time bin have not been averaged.

SUPPORTING INFORMATION

Additional Supporting Information may be found in the online version of this article:

Appendix A. Description (http://mnras.oxfordjournals.org/lookup/suppl/doi:10.1093/mnras/stu529/-/DC1).

Please note: Oxford University Press is not responsible for the content or functionality of any supporting materials supplied by the authors. Any queries (other than missing material) should be directed to the corresponding author for the article.

This paper has been typeset from a TEX/LATEX file prepared by the author.